

# Journal of Visualized Experiments

## Serial Block-Face Scanning Electron Microscopy (SBF-SEM) of Biological Tissue Samples

--Manuscript Draft--

<b>Article Type:</b>	Invited Methods Article - JoVE Produced Video
<b>Manuscript Number:</b>	JoVE62045R1
<b>Full Title:</b>	Serial Block-Face Scanning Electron Microscopy (SBF-SEM) of Biological Tissue Samples
<b>Corresponding Author:</b>	Justin Courson University of Houston Houston, TX UNITED STATES
<b>Corresponding Author's Institution:</b>	University of Houston
<b>Corresponding Author E-Mail:</b>	jacourso@central.uh.edu
<b>Order of Authors:</b>	Justin Courson Paul Landry Thao Do Eric Spehlmann Pascal Lafontant Nimesh Patel Rolando Rumbaut Alan Burns
<b>Additional Information:</b>	
<b>Question</b>	<b>Response</b>
Please indicate whether this article will be Standard Access or Open Access.	Standard Access (US\$2,400)
Please indicate the <b>city, state/province, and country</b> where this article will be <b>filmed</b> . Please do not use abbreviations.	Houston, Texas, United States of America
Please confirm that you have read and agree to the terms and conditions of the author license agreement that applies below:	I agree to the <a href="#">Author License Agreement</a>
Please specify the section of the submitted manuscript.	Biology
Please provide any comments to the journal here.	



**1 TITLE:**

2 Serial Block-Face Scanning Electron Microscopy (SBF-SEM) of Biological Tissue Samples

**4 AUTHORS AND AFFILIATIONS:**

5 Justin A. Courson<sup>1</sup>, Paul T. Landry<sup>1</sup>, Thao Do<sup>1</sup>, Eric Spehlmann<sup>2</sup>, Pascal J. Lafontant<sup>2</sup>, Nimesh  
6 Patel<sup>1</sup>, Rolando E. Rumbaut<sup>3,4</sup>, Alan R. Burns<sup>1,4</sup>

7  
8 <sup>1</sup>University of Houston, College of Optometry, Houston, TX, United States of America

9 <sup>2</sup>DePauw University, Department of Biology, Greencastle, IN, United States of America

10 <sup>3</sup>Center for Translational Research on Inflammatory Diseases (CTRID), Michael E. DeBakey  
11 Veterans Affairs Medical Center, Houston, TX, United States of America

12 <sup>4</sup>Baylor College of Medicine, Children's Nutrition Center, Houston, TX, United States of America

13  
14 Email Addresses of Co-Authors:

15 Paul T. Landry (ptlandry@uh.edu)

16 Thao Do (thaodo927@gmail.com)

17 Eric Spehlmann (ericSpehlmann\_2021@depauw.edu)

18 Pascal Lafontant (pascallafontant@depauw.edu)

19 Nimesh Patel (nbpatel@central.uh.edu)

20 Rolando E. Rumbaut (rrumbaut@bcm.edu)

21 Alan R. Burns (arburns2@central.uh.edu)

22  
23 Corresponding Author:

24 Justin A. Courson (JACourso@central.uh.edu)

**26 KEYWORDS:**

27 Serial Block-Face Scanning Electron Microscopy, SBF-SEM, 3D-EM, 3D-Reconstruction, Tissue  
28 Preparation, Specimen Preparation, Serial Sections, Ultrastructure, High-resolution, Volumetric  
29 Imaging, Biological, Large Volume

**31 SUMMARY:**

32 This protocol outlines a routine method for using serial block-face scanning electron microscopy  
33 (SBF-SEM), a powerful 3D imaging technique. Successful application of SBF-SEM hinges on proper  
34 fixation and tissue staining techniques, as well as careful consideration of imaging settings. This  
35 protocol contains practical considerations for the entirety of this process.

**37 ABSTRACT:**

38 Serial block-face scanning electron microscopy (SBF-SEM) allows for the collection of hundreds  
39 to thousands of serially-registered ultrastructural images, offering an unprecedented three-  
40 dimensional view of tissue microanatomy. While SBF-SEM has seen an exponential increase in  
41 use in recent years, technical aspects such as proper tissue preparation and imaging parameters  
42 are paramount for the success of this imaging modality. This imaging system benefits from the  
43 automated nature of the device, allowing one to leave the microscope unattended during the  
44 imaging process, with the automated collection of hundreds of images possible in a single day.

45 However, without appropriate tissue preparation cellular ultrastructure can be altered in such a  
46 way that incorrect or misleading conclusions might be drawn. Additionally, images are generated  
47 by scanning the block-face of a resin-embedded biological sample and this often presents  
48 challenges and considerations that must be addressed. The accumulation of electrons within the  
49 block during imaging, known as “tissue charging,” can lead to a loss of contrast and an inability  
50 to appreciate cellular structure. Moreover, while increasing electron beam intensity/voltage or  
51 decreasing beam-scanning speed can increase image resolution, this can also have the  
52 unfortunate side effect of damaging the resin block and distorting subsequent images in the  
53 imaging series. Here we present a routine protocol for the preparation of biological tissue  
54 samples that preserves cellular ultrastructure and diminishes tissue charging. We also provide  
55 imaging considerations for the rapid acquisition of high-quality serial-images with minimal  
56 damage to the tissue block.

57

## 58 **INTRODUCTION:**

59 Serial block face scanning electron microscopy (SBF-SEM) was first described by Leighton in 1981  
60 where he fashioned a scanning electron microscope augmented with an in-built microtome  
61 which could cut and image thin sections of tissue embedded in resin. Unfortunately, technical  
62 limitations restricted its use to conductive samples, as non-conductive samples such as biological  
63 tissue accumulated unacceptable levels of charging (electron buildup within the tissue sample)<sup>1</sup>.  
64 While coating the block-face between cuts with evaporated carbon reduced tissue charging, this  
65 greatly increased imaging acquisition time and image storage remained a problem as computer  
66 technology at the time was insufficient to manage the large file sizes created by the device. This  
67 methodology was revisited by Denk and Horstmann in 2004 using a SBF-SEM equipped with a  
68 variable pressure chamber<sup>2</sup>. This allowed for the introduction of water vapor to the imaging  
69 chamber which reduces charging within the sample, making imaging of non-conductive samples  
70 viable albeit with a loss of image resolution. Further improvements in tissue preparation and  
71 imaging methods now allow for imaging using high vacuum, and SBF-SEM imaging no longer  
72 relies on water vapor to dissipate charging<sup>3-9</sup>. While SBF-SEM has seen an exponential increase  
73 in use in recent years, technical aspects such as proper tissue preparation and imaging  
74 parameters are paramount for the success of this imaging modality.

75

76 SBF-SEM allows for the automated collection of thousands of serially-registered electron  
77 microscopy images, with planar resolution as small as 3-5 nm<sup>10,11</sup>. Tissue, impregnated with heavy  
78 metals and embedded in resin, is placed within a scanning electron microscope (SEM) containing  
79 an ultramicrotome fitted with a diamond knife. A flat surface is cut with the diamond knife, the  
80 knife is retracted, and the surface of the block is scanned in a raster pattern with an electron  
81 beam to create an image of tissue ultrastructure. The block is then raised a specified amount  
82 (e.g., 100 nm) in the z-axis, known as a “z-step,” and a new surface is cut before the process is  
83 repeated. In this way a 3-dimensional (3D) block of images is produced as the tissue is cut away.  
84 This imaging system further benefits from the automated nature of the device, allowing one to  
85 leave the microscope unattended during the imaging process, with the automated collection of  
86 hundreds of images possible in a single day.

87

88 While SBF-SEM imaging primarily uses backscattered electrons to form an image of the block-

89 face, secondary electrons are generated during the imaging process<sup>12</sup>. Secondary electrons can  
90 accumulate, alongside backscattered and primary-beam electrons that do not escape the block,  
91 and produce “tissue charging,” which can lead to a localized electrostatic field at the block-face.  
92 This electron accumulation can distort the image or cause electrons to be ejected from the block  
93 and contribute to the signal collected by the backscatter detector, decreasing the signal-to-noise  
94 ratio<sup>13</sup>. While the level of tissue charging can be decreased by reducing the electron beam voltage  
95 or intensity, or reducing beam dwell time, this results in a diminished signal-to-noise ratio<sup>14</sup>.  
96 When an electron beam of lower voltage or intensity is used, or the beam is only allowed to dwell  
97 within each pixel space for a shorter period of time, less backscattered electrons are ejected from  
98 the tissue and captured by the electron detector resulting in a weaker signal. Denk and  
99 Horstmann dealt with this problem by introducing water vapor into the chamber, thereby  
100 reducing charge in the chamber and on the block face at the cost of image resolution. With a  
101 chamber pressure of 10-100 Pa, a portion of the electron beam is scattered contributing to image  
102 noise and a loss of resolution, however this also produces ions in the specimen chamber which  
103 neutralizes charge within the sample block<sup>2</sup>. More recent methods for neutralizing charge within  
104 the sample block use focal gas injection of nitrogen over the block-face during imaging, or  
105 introducing negative voltage to the SBF-SEM stage to decrease probe-beam-lading energy and  
106 increase signal collected<sup>6,7,15</sup>. Rather than introducing stage bias, chamber pressure or localized  
107 nitrogen injection to decrease charge buildup on the block surface, it is also possible to increase  
108 the conductivity of the resin by introducing carbon to the resin mix allowing for more aggressive  
109 imaging settings<sup>16</sup>. The following general protocol is an adaptation of the Deerinck et al. protocol  
110 published in 2010 and covers modifications to tissue preparation and imaging methodologies we  
111 found useful for minimizing tissue charging while maintaining high resolution image  
112 acquisition<sup>3,17-19</sup>. While the previously mentioned protocol focused on tissue processing and  
113 heavy metal impregnation, this protocol provides insight into the imaging, data analysis, and  
114 reconstruction workflow inherent to SBF-SEM studies. In our laboratory, this protocol has been  
115 successfully and reproducibly applied to a wide variety of tissues including cornea and anterior  
116 segment structures, eyelid, lacrimal and harderian gland, retina and optic nerve, heart, lung and  
117 airway, kidney, liver, cremaster muscle, and cerebral cortex/medulla, and in a variety of species  
118 including mouse, rat, rabbit, guinea pig, fish, monolayer and stratified cell cultures, pig, non-  
119 human primate, as well as human<sup>20-23</sup>. While small changes may be worthwhile for specific tissues  
120 and applications, this general protocol has proven highly reproducible and useful in the context  
121 of our core imaging facility.

122

## 123 **PROTOCOL:**

124

125 All animals were handled according to the guidelines described in the Association for Research  
126 in Vision and Ophthalmology Statement for the Use of Animals in Vision and Ophthalmic  
127 Research and the University of Houston College of Optometry animal handling guidelines. All  
128 animal procedures were approved by the institutions in which they were handled: Mouse, rat,  
129 rabbit, guinea pig, and non-human primate procedures were approved by the University of  
130 Houston Animal Care and Use Committee, zebrafish procedures were approved by the DePauw  
131 University Animal Care and Use Committee, and pig procedures were approved by the Baylor  
132 College of Medicine Animal Care and Use Committee. All human tissue was handled in

133 accordance with the Declaration of Helsinki regarding research on human tissue and appropriate  
134 institutional review board approval was obtained.

135

## 136 **1. Tissue Processing**

137

138 1.1. Prepare a stock solution of 0.4 M sodium cacodylate buffer by mixing sodium cacodylate  
139 powder in ddH<sub>2</sub>O. Thoroughly mix buffer and pH adjust the solution to 7.3. This buffer is used to  
140 make fixative (composition described below in step 1.3), washing buffer, as well as osmium and  
141 potassium ferrocyanide solutions.

142

143 NOTE: Perfusion fixation is often the best method of fixation for SBF-SEM studies, as fixation  
144 occurs rapidly and throughout the body. If perfusion fixation is not possible within your study  
145 design, skip to step 1.3.

146

147 1.2. Perform perfusion fixation with the appropriate physiological pressure for the animal  
148 model<sup>24-26</sup>. This is done via transcardial sequential perfusion with heparinized saline followed by  
149 fixative, each placed at a specific height (e.g., 100 cm) above the organism (appropriate to the  
150 physiological pressure of the vascular system in the animal model), with fixative flowing into the  
151 left ventricle, and exiting out of an incision made in the right atrium. Tissue of interest will  
152 become pale as blood is replaced with fixative, if all or a portion of your tissue does not blanch  
153 then tissue may not be appropriately fixed and ultrastructure may not be preserved.

154

155 1.3. Use a razor blade or sharp scalpel to trim tissue samples into blocks no larger than 2 mm  
156 x 2 mm x 2 mm. If step 1.2 was skipped, do this swiftly so that tissue can be immersion fixed as  
157 quickly as possible.

158

159 1.3.1. Alternatively, dissect tissue under fixative and transfer to fresh fixative to complete the  
160 immersion process. The final composition of the fixative consists of 0.1 M sodium cacodylate  
161 buffer containing 2.5% glutaraldehyde and 2 mM calcium chloride. Allow fixation to proceed for  
162 a minimum of 2 hours at room temperature and a maximum of overnight at 4 °C. If possible, use  
163 a rocker/tilt plate to gently agitate samples while fixing.

164

165 1.3.2. Alternatively, if an inverter microwave is available, fix tissue in aforementioned fixative  
166 under vacuum at 150 watts for 4 cycles of 1 minute on, 1 minute off. Microwave fixation is the  
167 preferred method for step 1.3 as it rapidly fixes tissue and preserves tissue ultrastructure<sup>27</sup>.

168

169 NOTE: Tissue should never be allowed to dry during this protocol, care should be taken to transfer  
170 tissue quickly from one solution to the next.

171

172 1.4. Wash fixed tissue 5x for 3 minutes each (15 minutes total) at room temperature in 0.1 M  
173 sodium cacodylate buffer containing 2 mM calcium chloride.

174

175 1.5. Make the following osmium ferrocyanide solution fresh, preferably during the previous  
176 wash steps. Combine a 4% osmium tetroxide solution (prepared in ddH<sub>2</sub>O) with an equal volume

177 of 3% potassium ferrocyanide in 0.2 M cacodylate buffer with 40 mM calcium chloride. After the  
178 previous wash step, place the tissue in this solution for 1 hour on ice in the dark, and in the fume  
179 hood.

180

181 NOTE: Osmium tetroxide is a yellow crystalline substance that comes in an ampule. To create the  
182 osmium tetroxide solution, crack open the ampule, add ddH<sub>2</sub>O, and sonicate for 3-4 hours in the  
183 dark until the crystals are completely dissolved. Osmium tetroxide solution is a clear yellow  
184 solution, if the solution is black the osmium has been reduced and should no longer be used.

185

186 1.6. While the tissue is incubating in the osmium ferrocyanide solution, begin preparing the  
187 thiocarbohydrazide (TCH) solution. Prepare this solution fresh and have it readily available at the  
188 end of the 1 hour osmium ferrocyanide fixation period. Combine 0.1 g of thiocarbohydrazide with  
189 10 mL of ddH<sub>2</sub>O and place this solution into a 60 °C oven for 1 hour. To ensure the solution is  
190 dissolved, gently swirl every 10 minutes. Prior to use, filter this solution through a 0.22 µm syringe  
191 filter.

192

193 1.7. Prior to incubating in TCH, wash the tissue with room temperature ddH<sub>2</sub>O 5x for 3 minutes  
194 each (15 minutes total).

195

196 1.8. Place the tissue in the filtered TCH solution for a total of 20 minutes at room temperature  
197 (**Figure 1A-C**).

198

199 1.9. Following incubation in TCH, wash the tissue 5x for 3 minutes each (15 minutes total) in  
200 room temperature ddH<sub>2</sub>O.

201

202 1.10. Place tissue in ddH<sub>2</sub>O containing 2% osmium tetroxide (not osmium reduced with  
203 potassium ferrocyanide) for 30 minutes at room temperature. This should be done in the fume  
204 hood and in the dark as osmium can be reduced by light (e.g., under aluminum foil) (**Figure 1D-**  
205 **F**).

206

207 1.11. Following osmium tetroxide incubation, wash tissue 5x for 3 minutes each (15 minutes  
208 total) in room temperature ddH<sub>2</sub>O.

209

210 1.12. Place tissue in 1% aqueous uranyl acetate (uranyl acetate powder mixed in ddH<sub>2</sub>O)  
211 overnight in a refrigerator at 4 °C.

212

213 1.13. Just before removing tissue from the refrigerator, prepare fresh Walton's lead aspartate  
214 solution. Begin by dissolving 0.066 g of lead nitrate in 10 mL of 0.03 M aspartic acid solution (0.04  
215 g aspartic acid in 10 mL of distilled water) and adjust pH to 5.5 with 1 N KOH (0.5611 g in 10 mL  
216 of distilled water).

217

218 CAUTION: A precipitate can form when adjusting the pH. This is not acceptable.

219

220 1.13.1. Using a stir bar, slowly add the 1 N KOH dropwise while monitoring pH. Pre-heat the

221 finished clear lead aspartate solution in a 60 °C oven for 30 minutes. If a precipitate forms the  
222 solution cannot be used and another solution must be prepared.

223

224 1.14. Remove the tissue from the refrigerator and wash 5x for 3 minutes each (15 minutes total)  
225 in room temperature ddH<sub>2</sub>O.

226

227 1.15. After washing, place the tissue in the warmed Walton's lead aspartate solution for 30  
228 minutes while maintaining the temperature at 60 °C.

229

230 1.16. After incubation in Walton's lead aspartate, wash the tissue 5x for 3 minutes each (15  
231 minutes total) in room temperature ddH<sub>2</sub>O (**Figure 1G-I**).

232

233 1.17. Dehydrate the tissue through an ice-cold acetone series (30%, 50%, 70%, 95%, 95%, 100%,  
234 100%, and 100% acetone (in ddH<sub>2</sub>O where applicable) allowing 10 minutes for each step in the  
235 series.

236

237 1.18. Following the ice-cold dehydration series, place tissue in room temperature acetone for  
238 10 minutes.

239

240 1.18.1. During this time, formulate Embed 812 ACM resin. Use the "hard mix" recipe as it is more  
241 resistant to beam damage. Mix the resin thoroughly, and place the tissue into Embed  
242 812:acetone (1:3 mix) for 4 hours, followed by Embed 812:acetone (1:1 mix) for 8 hours or  
243 overnight, and finally Embed 812:acetone (3:1 mix) overnight. Perform these resin-embedding  
244 steps at room temperature.

245

246 1.19. The next day, place the tissue in 100% Embed 812 for 4-8 hours, then in fresh 100% Embed  
247 812 overnight, and finally into fresh 100% Embed 812 for 4 hours. Perform these resin-  
248 embedding steps at room temperature.

249

250 1.19.1. Just before embedding, place a small amount of resin into a mixing container and slowly  
251 mix (a wooden stick can be used for stirring) in carbon black powder until the resin is saturated  
252 with the powder but is still fluid and does not become grainy. It should resemble thick ink and be  
253 able to slowly drip from the wooden stick without visible clumps.

254

255 1.20. Orient the tissue samples in a silicone rubber mold and take a picture so that sample  
256 orientation within the resin block is recorded and can be referenced. Cover the samples in carbon  
257 black saturated resin at the tip of the silicone mold and place the mold in an oven for ~1 hour at  
258 65 °C.

259

260 1.20.1. Place the mold at an incline to contain the resin at the tip of the mold where it covers the  
261 tissue sample. Place a label with an experiment/tissue sample identifier in the mold at the  
262 opposite end of the resin (**Figure 2A**).

263

264 1.21. Remove the silicone mold from the oven and fill the remainder of the mold with clear

265 resin (no carbon black) making sure that the label remains visible. Cure the resin infused with  
266 carbon black enough as to not readily mix with the clear resin.

267  
268 1.21.1 Prepare an extra well within the mold that does not contain tissue. Beginning with the  
269 extra well, fill the remainder of the mold with clear resin.

270  
271 1.21.2 If the carbon black infused resin begins to bleed into the clear resin, place the silicone  
272 mold back into the oven for additional time (e.g., 15 minutes).

273  
274 1.21.3 Once all of the tissue samples have been topped off with clear resin, place the silicone  
275 mold back into the oven (flat, no incline) at 65 °C for 48 hours to complete the curing process.

276

## 277 2 Block Preparation

278

279 NOTE: The method will depend on how the sample is oriented in the block and how the sectioning  
280 is to take place. However, the most common tissue orientation finds the tissue centered in the  
281 tip of the resin block, perpendicular to the long end of the resin block.

282

283 2.21 In most cases, first trim the end of the block to locate the tissue by placing the specimen  
284 block in the microtome chuck with the tapered end sticking up approximately 5-6 mm out of the  
285 chuck. Lock it in place with the set screw and place it under a heat lamp.

286

287 2.22 After several minutes the block will be malleable and easy to trim. Place the chuck in the  
288 stereomicroscope holder and use a new double-edge razor blade to make thin sections parallel  
289 with the block face until the tissue is visible. This is best seen by angling light across the block  
290 face, the tissue sample will be less reflective and granular compared to those portions of the resin  
291 that are devoid of tissue. Consult the photograph taken of tissue samples prior to introduction of  
292 carbon black saturated resin for an idea of how and where the tissue is located.

293

294 2.23 Set one specimen pin holder aside for trimming purposes. This pin holder is never placed  
295 into the SEM chamber and can therefore be handled without gloves, this will be referred to as  
296 the trimming pin holder. **Any specimen holder destined to be placed into the imaging chamber  
297 should never be touched without gloves. This avoids introducing grease and oil into the  
298 microscope chamber.**

299

300 2.24 Place an aluminum specimen pin in the trimming pin holder and slightly tighten the set  
301 screw with the face (flat surface) of the pin held 3-4mm above the pin holder.

302

303 2.25 Make several deep, crisscrossing scratches in the face of the pin to provide a larger  
304 surface area for the glue used to hold the specimen in place. If an aluminum pin is used, a small  
305 steel flathead screwdriver is recommended for this step (**Figure 2B**).

306

307 2.26 Place the chuck containing the tissue sample back under the heat lamp until the resin  
308 becomes soft and malleable, then place it into the chuck-receptacle under the stereomicroscope.

309

310 2.27 Using a double-edged razor blade to trim away excess resin from the portion of the resin  
311 block containing the tissue sample. Ultimately the size of tissue block attached to the pin will be  
312 approximately 3 mm in diameter and 2-3 mm in height.

313

314 2.27.1. Carefully push the razor straight down into the resin block roughly 1-2 mm, then carefully  
315 push the razor horizontally into the resin block at a depth equal to the previous cut. Do this slowly  
316 and with great care, as it is possible to damage or cut away the portion of the block containing  
317 the tissue sample. As the two cuts meet, the excess resin will separate from the block. Continue  
318 to remove resin until only a 3 mm x 3 mm raised area remains.

319

320 2.28 After this initial trimming, place the block (still in the chuck) under the heat lamp for  
321 several minutes.

322

323 2.29 Once the resin becomes soft and malleable, place the block back under the  
324 stereomicroscope. Using a new double-edge razor blade, cut off the top of the resin block,  
325 roughly 1 mm below the trimmed portion, with a single smooth cut. A flat surface is preferable  
326 as this will be glued to the specimen pin. Be careful not to allow the sample to become lost, as  
327 this step requires some force which can transfer to the removed portion of the block and cause  
328 it to fly away. Place the cut and trimmed sample aside.

329

330 2.30 Place the trimming pin holder containing the cut aluminum pin in the stereomicroscope  
331 receptacle. Apply a thin layer of cyanoacrylate glue to the pin face such that it completely covers  
332 the pin without forming a visible meniscus. Pick up the trimmed piece of the tissue block with  
333 forceps and place in on the pin face. Center the tissue sample on the specimen pin. Push it down  
334 and hold it for several seconds. Allow the glue to set for several minutes.

335

336 2.31 When the glue is thoroughly dry, place the trimming pin holder back under the  
337 stereomicroscope. Using a fine file, file away excess resin so that no resin is overhanging the pin.  
338 The resin shape should resemble the circular pin head.

339

340 2.32 Locate the tissue on the raised portion of your resin block, oblique lighting is useful for  
341 this. Using a double-edge razor, the raised portion of the resin containing the tissue sample must  
342 be trimmed to an area no larger than 1 mm<sup>2</sup>. If possible, the block-face can be trimmed even  
343 smaller, this will reduce stress on the diamond knife and improve its longevity.

344

345 2.32.1. Remove as much excess resin as possible, leaving the block slightly longer in one  
346 dimension. This is done slowly and with care, as it is possible for the resin containing the tissue  
347 sample to break away if too much force is applied. While a razor is recommended, a fine metal  
348 file can be used for this step.

349

350 2.33 With a fine metal file angle the excess resin, in the area outside the raised portion  
351 containing the tissue sample, down towards the edge of the pin (**Figure 2C**).

352



353 2.34 Remove resin particles and dust from the prepared sample before applying silver paint  
354 followed by gold sputtering. Mix silver with acetone so that it is an easily spreadable liquid, akin  
355 to nail polish (but not so thin that it drips off of the applicator) and apply a thin coat to the entire  
356 sample block surface. Acetone evaporates rapidly, so it may be necessary to add additional  
357 acetone as the silver paint begins to thicken.

358

359 2.34.1 Allow the silver paint to dry overnight before loading into the microscope.

360

361 NOTE: This silver layer must be thin in order to avoid expanding the block-face beyond 1 mm x 1  
362 mm, and while the silver paint has never damaged the diamond knife, smaller block-faces are still  
363 recommended to preserve the longevity of the diamond knife. The acetone mixed in with the  
364 silver must evaporate completely before gold-sputtering or loading the sample into the  
365 microscope to avoid introducing acetone vapor into the imaging chamber.

366

367 2.34.2 Following application of silver paint, apply a thin layer of gold to the sample block. Using  
368 a standard vacuum sputtering device equipped with a standard gold foil target, a chamber  
369 pressure of 200 milli Torr (Argon gas) and 40 milliamps running for 2 minutes will result in a 20  
370 nm thick gold coating.

371

372 2.35 After coating, place the mounted and trimmed block in a tube with the appropriate  
373 experiment label attached. Create custom tubes using disposable transfer pipettes.

374

375 2.35.1. Cut the transfer pipette just below the bulb, leaving a short portion of the transfer pipette  
376 tube attached below the bulbous end. Shorten the tubular portion that was cut away, and cut  
377 the pipette tip back enough so that the aluminum specimen pin can be pushed snugly inside of  
378 it.

379

380 2.35.2. Place the end containing the aluminum specimen pin within the bulbous end of the  
381 modified transfer pipette.

382

383 2.36 Before loading a prepared tissue block, carefully trim away excess silver paint from the  
384 surface of the block face.

385

### 386 **3 SEM Settings for Imaging the Block Face**

387

388 NOTE: The imaging settings that follow were produced on the device used by the authors, which  
389 is listed in the **Table of Materials** provided. While this device is capable of variable pressure  
390 imaging, best results were captured under high vacuum.

391

392 **3.21 Dwell Time:** Use 12  $\mu\text{s}/\text{px}$  during serial sectioning. When a region of interest has been  
393 identified, a higher resolution image can be acquired at 32  $\mu\text{s}/\text{px}$ .

394

395 **3.22 Vacuum Settings:** Use a gun pressure of 9e-008 Pa, a column pressure of 1.1e-004 Pa, and  
396 a chamber pressure of 9.5e-002 Pa.

397

398 **3.23 Capture Time:** With the above settings, capture a 2048x2048 px image stack at a rate of  
399 50 seconds per image. Higher resolution images of regions of interest can be captured at  
400 4096x4096 px at just under 9 minutes per image.

401

402 **3.24 Section Thickness:** Use 100-200 nm. Less is possible, but may require lower beam voltage,  
403 intensity, or dwell time.

404

405 **3.25 High Voltage (HV):** Use 7-12 kV. While increasing the voltage reduces the spot size and  
406 increases resolution, it introduces more possibility for beam damage. Higher kV increases the  
407 beam penetration which results in loss of details. However, lowering the kV degrades the signal  
408 to noise ratio (**Figure 3**)<sup>14</sup>.

409

410 **3.26 Beam Intensity (BI):** The author's SBF-SEM device offers a beam intensity scale ranging  
411 from 1-20. On this scale, values of 5-7 give quality images without excessive charging and beam  
412 damage. The higher the BI the greater the resolution however, there is more chance of charging  
413 and beam damage<sup>14</sup>.

414

415 **3.27 Spot Size and Image Magnification:** Determine the spot size by the beam intensity and  
416 voltage level. Ideally, the spot size should not be larger than the pixel size used. The pixel size is  
417 determined by dividing the field of view (FOV) by the number of pixels. For example, a 25  $\mu\text{m}$   
418 FOV with an image size of 2048x2048 px would give 12.2 nm per pixel. Therefore spot size should  
419 be no greater than 12.2 nm. **Figure 4** shows how HV, BI and spot size are related.

420

421 **3.28 Working Distance (WD)** – With block face imaging the working distance is not adjustable.  
422 It is simply a factor of focus. It will be nearly identical for all blocks imaged. While the working  
423 distance is not adjustable, it plays a critical role in the resolution of the image captured. As  
424 working distance decreases, the resolution limit on images captured increases. In some cases it  
425 may be possible to decrease the working distance by making modifications within the imaging  
426 chamber, however these modifications must be made at the user's discretion. In order to  
427 decrease the working distance and increase image resolution, we loosened the door mount  
428 microtome screws and repositioned the microtome so that it rested  $\sim 2$  mm closer to the beam  
429 detector after retightening the screws.

430

431 **3.29 Resolution** – Using the above settings, x & y resolution as high as 3.8 nm is possible. It is  
432 important to note that resolution is limited by beam spot size as well as the pixel resolution of  
433 the image captures (e.g., a 20  $\mu\text{m}$  field of view captured in a 2048x2048 pixel image has a pixel  
434 resolution of 9.8 nm, even if a 3.8 nm spot size was used). Image resolution in the z-plane is  
435 dependent on sectioning thickness, we find that 100-200 nm works well with this protocol.

436

## 437 **REPRESENTATIVE RESULTS:**

438 Mouse Cornea

439 This protocol has been applied extensively to the mouse cornea. Using SBF-SEM imaging a  
440 network of elastin-free microfibril bundles (EFMBs) were shown to be present within the adult

441 mouse cornea. It was previously believed that this network was only present during embryonic  
442 and early postnatal development. SBF-SEM revealed an extensive EFMB network throughout the  
443 cornea, with individual fibers found to be 100-200 nm in diameter when measured in cross-  
444 section. It was also found that this EFMB network was organized in distinct layers, with fibers  
445 closely associated with keratocytes, even lying within shallow invaginations on the keratocyte  
446 surface (**Figure 5**). The discovery of EFMB fibers in the adult cornea led to immunogold-labeling  
447 transmission electron microscopy (TEM), fluorescence and confocal studies to further  
448 understand the nature of this network<sup>23</sup>.

449  
450 Further application of this protocol led to the discovery of a previously unknown population of  
451 central corneal nerves that fuse with basal epithelial cells at the stromal-epithelial border (**Figure**  
452 **6**). Previously, it was believed that all nerves interacting with the epithelium at this border  
453 penetrated into the corneal epithelium and ramified producing the subbasal and epithelial plexi.  
454 In this study, ~45% of central nerves interacting with the basal epithelium underwent cell-cell  
455 fusion rather than simple penetration. Using stereological methods applied to SBF-SEM data sets,  
456 it was possible to show this novel nerve population had a surface-to-volume ratio roughly half  
457 that of penetrating nerves, consistent with their “swollen” appearance (Nerve Fusion -  $3.32 \pm 0.25$ ,  
458 Nerve Penetration -  $1.39 \pm 0.14$ ,  $p \leq 0.05$ ). 3D reconstructions of penetrating and fusing nerve  
459 bundles and their mitochondria were created, highlighting the lack of mitochondria in fused  
460 portions of the nerve bundles. The discovery of neuronal-epithelial cell fusion using SBF-SEM led  
461 to fluorescence studies verifying membrane continuity between the two fused cells<sup>21</sup>.

462  
463 The central cornea is an avascular tissue, and as such the peripheral limbal vasculature is of  
464 particular importance to the overall health of the cornea. The cell-cell relationships and  
465 ultrastructure of this region is complex; however, the ability to appreciate these cell-cell  
466 interactions and ultrastructural connections has been limited in fluorescence and single section  
467 TEM studies. For this reason an SBF-SEM image stack containing limbal vasculature, nerve  
468 bundles, and associated cells was manually segmented for 3D reconstruction (**Figure 7**). In this  
469 image the close association between vascular endothelial junctions and an overlaying pericyte,  
470 the individual granules of a perivascular mast cell, the nucleus and leading edge of a neutrophil  
471 crawling along the outer surface of the blood vessel wall, as well as a passing nerve bundle can  
472 be seen.

473  
474 Taken together, this body of work demonstrates the capability of this protocol to produce high  
475 quality 3D electron microscopy data sets in tissues rich in extracellular matrix and epithelium, as  
476 well as vasculature and associated cells.

477  
478 Higher Order Primate Retina – Nerve Plexus and Vascular Network  
479 The retinal nerve fiber layer (RNFL) of higher order primates contains and depends on an  
480 extensive vascular network. Often, diseases of the retina involve changes in both parameters of  
481 the retinal nerve fiber layer as well as the vasculature found within it. Understanding the  
482 relationship between the RNFL and its vascular network in healthy, non-pathological tissue is the  
483 first step to understanding any changes that may occur as a result of disease. In order to better  
484 understand this relationship, the SBF-SEM protocol was applied to normal higher order primate

485 retina and the reconstruction of the vascular network was performed and volumetric data  
486 extracted from this reconstruction (**Figure 8**). This 4,642,307  $\mu\text{m}^3$  region of the RNFL contained a  
487 vascular bed  $1.207 \times 10^{-4}$   $\mu\text{L}$  in volume, making up 2.6% of the total volume of the RNFL. This work  
488 demonstrates the capability of this protocol to produce high quality 3D electron microscopy data  
489 sets in dense neurological tissue.

490

#### 491 Zebrafish and Giant Danio Heart – Striated Muscle and Developing Vasculature

492 Both the zebrafish and the giant danio are important models for heart development and  
493 regeneration. Historically, the zebrafish heart is considered to consist of two anatomically distinct  
494 myocardial segments functioning together in support of the physiological demands of the  
495 zebrafish. However, the interface between these two ventricular layers was not well understood.  
496 Using this protocol, a previously unrecognized junctional region was discovered consisting of a  
497 thin sheet of fibroblasts. It was found that openings within this sheet allowed two separate  
498 myocardial segments to come into contact and form complex adhesions junctions including  
499 desmosomes and fascia adherens<sup>22</sup>.

500

501 This protocol has been utilized in further work examining the vascular network of the developing  
502 giant danio heart (**Figure 9**). This method allows for the 3D appreciation of the developing cardiac  
503 myocyte network and its relationship with developing microvasculature. Taken together, this  
504 work demonstrates the capability of this protocol to produce high quality 3D electron microscopy  
505 data sets in muscle and highly vascularized tissues.

506

#### 507 Image Settings, Charging, and Resolution

508 While appropriate fixation and heavy metal staining is necessary for quality SBF-SEM imaging,  
509 equally important is the use of conductive resin and proper imaging settings for the questions  
510 being addressed. In this protocol, the use of carbon black is employed in order to increase the  
511 conductivity of the sample block and provide a conduit to the mounting pin for the clearance of  
512 secondary electrons from the block-face. This has proven effective in combatting tissue charging  
513 which often degrades image quality in tissues not prepared with carbon black<sup>16</sup>. In addition, the  
514 silver paint and gold sputtering applied to the block provides a dissipation pathway for electron  
515 buildup. Some devices allow for the addition of a focal charge compensator, which reduces  
516 charging by applying a puff of nitrogen over the block-face, however we have had similar success  
517 with the use of carbon black and the application of silver paint and gold sputtering to the block<sup>15</sup>.  
518 Lack of sample conductivity can lead to electron buildup visible as tissue charging (**Figure 1**), as  
519 well as discharges that are visible as abrupt image shifting and warping which dramatically  
520 diminish image quality (**Figure 10B & F**). The use of carbon black allows for imaging under high-  
521 vacuum and the use of image settings that result in high signal-to-noise ratio and improved image  
522 resolution. One such setting that leads to improved image quality is pixel dwell time. The SBF-  
523 SEM imaging process involves the raster scanning of an electron beam across the sample surface  
524 to generate backscattered electrons which the microscope detector can collect and interpret as  
525 signal. The length of time this beam is allowed to dwell within the space of each pixel leads to a  
526 more accurate pixel value being assigned to each pixel location (**Figure 3A & B**)<sup>2</sup>. There is a  
527 balance that must be struck between increased signal-to-noise, resolution and damage dealt to  
528 the block-face however. The beam effectively irradiates the block-face with high energy electrons

529 which can break down and soften resin resulting in image degradation and cutting complications  
530 (**Figure 10**)<sup>28</sup>. The thinner the z-resolution required, the more difficult it becomes to maintain  
531 high-resolution imaging. We generally use z-steps of 100-200 nm, however z-step sizes of 25-50  
532 nm have been reported<sup>5,29-31</sup>. With z-steps of this size, the break-down and softening of resin due  
533 to beam damage can lead to either compression of the resin causing the knife to miss a cut or  
534 cut the block-face but with “chatter” where the knife skips across the surface of the block creating  
535 ripples and bands<sup>13</sup>. While small z-steps are an attractive prospect, it is important to keep the  
536 specific research question in mind when choosing an appropriate z-step. Over-sampling can lead  
537 to substantial data-storage considerations as well as an increase in time required to produce 3D  
538 reconstructions.

539

#### 540 Tissue fixation and Staining

541 Prior to heavy metal incubation, tissues must be fixed in glutaraldehyde. While we highly  
542 recommend microwave fixation under vacuum for the preservation of tissue ultrastructure<sup>27</sup>, if  
543 a laboratory grade microwave is not available a commercial inverter microwave with variable  
544 wattage can be substituted<sup>32-35</sup>. If this is done, extra care should be employed to ensure that  
545 tissue distortion does not occur. Improper tissue fixation can result in altered tissue morphology  
546 as can be seen in **Figure 10E**. This protocol, like most modern SBF-SEM staining protocols, has  
547 been adapted from the staining procedure outlined by Deerinck in 2010<sup>17</sup>, based on the osmium-  
548 thiocarbonylhydrazide-osmium stains created by Willingham and Rutherford in 1984<sup>36</sup>. The heavy  
549 metals utilized in this protocol add contrast to the cellular structures within a tissue sample  
550 (**Figure 1**). The initial osmium incubation occurs with reduced osmium which binds to C=C bonds  
551 in unsaturated fats leading to membrane and lipid staining<sup>37,38</sup>. Osmium is reduced by potassium  
552 ferrocyanide, which assists in the staining of saturated lipids and also acts to stabilize  
553 phospholipids<sup>39,40</sup>. Thiocarbonylhydrazide is subsequently added as a mordant that binds to the  
554 osmium from the first incubation, acting as a bridge on which further osmium is bound at a later  
555 stage in the protocol<sup>41</sup>. Uranyl acetate, which is a uranium salt, is an effective contrasting agent  
556 for lipids, nucleic acids and proteins, while lead citrate enhances contrast of proteins and  
557 glycogens. The varying affinities of these agents for cellular components further enhances the  
558 overall contrast within tissues over and above the osmium incubations<sup>42</sup>.

559

#### 560 Imaging the Block-Face

561 **Figures 11-13** illustrate the combined effects of voltage, pixel dwell time and beam intensity.  
562 Conventional practice suggests a combination of low voltage, short dwell time and low beam  
563 intensity are necessary for optimal imaging and preventing beam damage to the sample block.  
564 Contrary to these settings, **Figures 11-13** illustrate that higher voltages (e.g., 7 kV), longer dwell  
565 times (32  $\mu$ s/px) and higher beam intensities (setting 6 in our case) can produce superior image  
566 quality over conventional settings.

567

568 SBF-SEM allows for the collection of serial electron microscopy images which can be collected as  
569 a 3D data set comprised of voxels. While this is an incredibly powerful use of SBF-SEM, this  
570 method also allows for the rapid and repeatable imaging of rare biological events or cells. Image  
571 acquisition using SBF-SEM can be monitored for rare events, and imaging paused in order to  
572 collect higher magnification/resolution images of these events. Furthermore, the block can be

573 removed from the microscope chamber and the block-face sectioned for transmission electron  
574 microscopy (TEM) imaging. In this way large datasets of rare events can be collected using SBF-  
575 SEM as well as appreciated at the angstrom scale using TEM.

576

577 **FIGURE LEGENDS:**

578 **Figure 1: SBF-SEM and TEM comparisons at various steps in the protocol.** This protocol contains  
579 multiple steps in which sample tissue is stained with heavy metals. This affects not only tissue  
580 contrast and appreciation of cellular structures and organelles, but also the levels of charging  
581 that occurs when the tissue is imaged. This figure contains three distinct views of prepared tissue:  
582 a low magnification view (**A, D & G**), a high magnification view (**B, E & H**), and a TEM comparison  
583 of prepared mouse cornea (**C, F & I**). It can be noted that higher magnification images can result  
584 in increased tissue charging, as the electron beam is concentrated in a smaller region of tissue.  
585 The top row (**A-C**) is a representative sample from tissue processed through the completion of  
586 step 1.8, and has been impregnated with potassium ferrocyanide, osmium tetroxide, and  
587 thiocarbonylhydrazide. The arrows in the first two columns show the epithelial-stromal interface as  
588 a reference point. Note the low level of contrast in comparison to the bottom two rows, as well  
589 as the increased levels of tissue charging. The sample in the middle row (**D-F**) was processed  
590 through the completion of step 1.10 and benefits from an additional osmium tetroxide step, and  
591 is visibly more contrasted than the sample in the top row. While cellular structures are  
592 discernible, charging is still present. The sample in the bottom row (**G-I**) benefits from the full  
593 staining protocol and has minimal tissue charging. TEM imaging reveals tissue contrast levels  
594 imparted by the heavy metals present at each step (right column): organelles in the corneal  
595 endothelium (\*) are more contrasted and apparent as tissue processing continues through the  
596 protocol. Additionally, stromal collagen and fibrillin details become more visible (arrowhead) as  
597 the protocol is completed. Panel A, D & G scale bar = 50  $\mu\text{m}$ . Panel B, E & H scale bar = 10  $\mu\text{m}$ .  
598 Panel C, F & I scale bar = 1  $\mu\text{m}$ .

599

600 **Figure 2: Schematic of embedded tissue block, specimen pin, and final preparation.** (**A**) Tissue  
601 should be placed in a known orientation at the very tip of the resin mold and the upper third of  
602 the mold filled with carbon black saturated resin. The region of the mold furthest from the tissue  
603 should remain clear so that the experiment label can be clearly seen. (**B**) Specimen pin surface  
604 should be scratched to produce a grid pattern, this allows for a greater area of contact for the  
605 cyanoacrylate glue to harden between the prepared specimen block and pin. (**C**) The carbon black  
606 saturated resin should make a wide area of contact with the specimen pin head, however the  
607 region that is cut by the diamond knife should be no greater than 1x1 mm. It is good practice to  
608 taper the block towards the tip. This minimizes cutting forces on the diamond knife and by having  
609 a wider base, the block is more resistant to separating from the pin during sectioning.

610

611 **Figure 3: Comparison of image capture settings.** (**A & B**) Panels **A** and **B** compare image quality  
612 and resolution as a function of pixel dwell time. Panel **A** was created using a 32  $\mu\text{s}$ /pixel dwell  
613 time at 4 kV and suffers from a diminished signal to noise ratio as is apparent in the “grainy”  
614 appearance of the enlarged inset. Panel **B** was created using a 100  $\mu\text{s}$ /pixel dwell time at 4 kV.  
615 Increasing the pixel dwell time increases the signal to noise ratio and reveals an increased level  
616 of cellular detail, however increased pixel dwell time has the potential to lead to tissue charging

617 and/or heat build-up which softens the block and introduces cutting artefacts (chatter) when  
618 sectioning. Panels **C** and **D** compare images captured under identical exposure conditions but  
619 with two different beam kV values. Tissue in these panels was impregnated with gold-toned  
620 nanogold particles to make differences in beam-penetration depths more apparent. Panel **C** was  
621 captured at 9 kV while panel **D** was captured at 21 kV. Increased kV has the advantage of  
622 increased contrast (**D**), however details are lost as result of gathering electrons from a greater  
623 depth of tissue (**C**). As a result of sampling a larger cross section, larger numbers of immunogold  
624 particles specific for GAP 43 are visible while non-specific labeling remains the same resulting in  
625 an increased signal-to-noise ratio. Panel A & B scale bar = 2  $\mu\text{m}$ . Panel C & D scale bar = 1  $\mu\text{m}$ .

626

627 **Figure 4: Beam intensity, kV and spot size.** (A) Upon contacting the tissue sample, the electron  
628 beam (light blue) yields a teardrop-shaped interaction volume, from which varying forms of  
629 energy are produced from the interaction between beam electrons and the tissue sample. The  
630 teardrop shape is a function of tissue density and heavy metal staining along with beam energy,  
631 and the tilt angle of the electron beam<sup>43</sup>. While x-rays, auger electrons, and tertiary electrons are  
632 produced during SBF-SEM imaging, the primary concern is with backscattered (dark blue) and  
633 secondary (green) electrons<sup>13</sup>. The image produced with SBF-SEM imaging is produced by  
634 collecting backscattered electrons. These electrons originate from elastic interactions between  
635 the beam and the sample, and the signal collected is highly dependent on the atomic number of  
636 atoms interacted with – hence the need for heavy metal staining<sup>44</sup>. Secondary electrons originate  
637 from inelastic interactions between the beam and the sample and detection of their signal is  
638 highly dependent on surface orientation. Because the block-face is flat in SBF-SEM, secondary  
639 electrons do not contribute meaningfully to the signal collected<sup>13</sup>. In fact, secondary electron  
640 accumulation on the surface of the block can be a major source of charging and has a deleterious  
641 effect on image quality<sup>2</sup>. (B) This graph shows the relationship between beam intensity, beam  
642 kV, and spot size. The spot size is the spatial resolution of the beam, and determines the  
643 resolution limit of the images being produced. Lowering kV increases the spot size, but also  
644 decreases the imaging depth allowing for finer appreciation of detail. This has the effect of  
645 decreasing the detectable signal as well. Increasing beam intensity offers an initial improvement  
646 on spot size and signal detection, but rapidly increases levels of tissue charging. Ultimately, the  
647 beam intensity and kV values chosen are sample dependent and best determined empirically in  
648 relation to the scientific question being asked.

649

650 **Figure 5: Elastin-free microfibril bundle network in the mouse cornea.** 3D reconstruction of  
651 microfibrils (white) closely associated with keratocytes (yellow, orange & green) within the  
652 corneal stroma. The microfibrils can be seen adjacent to, and in some cases within shallow  
653 grooves in, corneal keratocytes (arrows) (A). This network of elastin-free microfibrils are  
654 organized in distinct layers within the corneal stroma (B). Scale bar = 2  $\mu\text{m}$ . The image block  
655 reconstructed is 45x45  $\mu\text{m}$  in the x & y axis, and 30  $\mu\text{m}$  in the z axis with voxel a resolution of  
656 22x22x100 nm.

657

658 **Figure 6: Reconstruction of corneal nerves passing through basal lamina at the stromal-**  
659 **endothelial border.** 3D reconstruction of a penetrating nerve (purple) as it passes through the  
660 basal lamina (green). This nerve can be seen to bifurcate prior to penetration. After penetrating

661 into the epithelium, both nerve branches underwent ramification. Mitochondria (yellow) are  
662 visible in the stromal and epithelial portions of the nerve bundle. Scale bar = 2.5  $\mu\text{m}$ . The image  
663 block reconstructed is 25x25  $\mu\text{m}$  in the x & y axis, and 14  $\mu\text{m}$  in the z axis with a voxel resolution  
664 of 12x12x100 nm.

665

666 **Figure 7: Limbal vasculature and associated cells in the peripheral mouse cornea.** A single image  
667 (A) from a 3D image block (B) can be seen through which a vessel, nerve bundle, and associated  
668 cells travel. Panel C shows a reconstructed vessel (red) with an associated pericyte (gray)  
669 wrapped around it covering the endothelial cell junctions. A nerve bundle (blue) bifurcates in  
670 close proximity to this vessel as it travels through the tissue. A neutrophil (yellow) can be seen  
671 parallel to the long axis of the vessel, with its polymorphic nucleus visible within its cell body and  
672 the trailing uropod visible as a protrusion towards the right of the image. A mast cell (magenta)  
673 is visible on the underside of the vessel. Panel D isolates this mast cell, where its granules (green)  
674 can be more easily seen overlaying the nucleus (purple) within the cell. Panel E highlights the  
675 cellular structures overlaid on the cellular reconstructions, with endothelial nuclei denoted in  
676 blue, and adherent microparticles visible in the vessel lumen (orange). Arrows show cell-cell  
677 borders between endothelial cells, which can be further seen as raised ridges extending along  
678 the cells on the luminal side of the vessel. Panel A scale bar = 2  $\mu\text{m}$ . The image block used to  
679 reconstruct these cells is 30x30  $\mu\text{m}$  in the x & y axis, and 42.5  $\mu\text{m}$  in the z axis with a voxel  
680 resolution of 14.6x14.6x100 nm.

681

682 **Figure 8: Reconstructed vascular network of the non-human primate retinal nerve fiber layer.**  
683 (A) A 200x200  $\mu\text{m}$  SBF-SEM image of the primate retina taken at 8192x8192 px. The location  
684 sampled is ~500 microns from the inferior temporal rim margin of a healthy eye with no  
685 pathology. The image series reconstructed in panels C & D were captured at 2048x2048 px, with  
686 imaging paused so that regions of interested could be imaged at 8192x8192 px. Panel B is the  
687 inlayed region of panel A, taken directly from the original image. Note the large number of axons  
688 and their mitochondria. (C) Orthoslice section through a 200x200x200  $\mu\text{m}$  tissue volume of a  
689 control eye inferior temporal nerve fiber layer, with vasculature segmented. (D) Z-projection of  
690 the nerve fiber layer vasculature. This series illustrates the resolution possible in a large field  
691 using this methodology. Panel A scale bar = 20  $\mu\text{m}$ . Panel B scale bar = 2  $\mu\text{m}$ . Image series voxel  
692 resolution is 97.6x97.6x500 nm. Region of interest pixel resolution is 24.4x24.4 nm.

693

694 **Figure 9: Segmentation and 3D volume rendering of vessels in the giant danio (*Devario***  
695 ***malabaricus*) compact heart.** (A) Two-dimensional micrograph in an image stack, showing the  
696 profile of a central venular-size vessel (arrow) and an endothelial nucleus (arrowhead), with  
697 surrounding cardiac myocytes rich in mitochondria and well organized sarcomeres (\*). (B) Two-  
698 dimensional micrograph of the image stack with a capillary-size vessel (arrow). (C) Biorthogonal  
699 projections of the micrograph stack showing the capillary in panel B projected through one  
700 orthogonal slice. (D) 3D rendering of segmented endothelial cells lining the reconstructed vessel.  
701 Illustrated in green, red, blue, and purple are four separate endothelial cells; the endothelial cell  
702 depicted in blue can be seen in cross section in panel B (arrow), while the endothelial cells  
703 depicted in red (arrow) and green (arrowhead) are seen in cross section in panel A. Panels A & B  
704 scale bar = 2  $\mu\text{m}$ . The image block reconstructed is 30x30  $\mu\text{m}$  in the x & y axis, and 16  $\mu\text{m}$  in the



705 z axis with a voxel resolution of 14.6x14.6x100 nm.

706

707 **Figure 10: Imaging complications and artefacts.** (A) The wavy and distorted nature of this image  
708 is the result of imaging using a pixel dwell time that is too long. This heats the resin block, leaving  
709 the block face soft and rubbery which results in a distorted image upon cutting. (B) This image  
710 contains a host of artefacts. The asterisk indicates a wavy distortion caused by prior imaging at a  
711 higher magnification and similar to panel A, concentrating the beam on a smaller region with a  
712 longer pixel dwell time has softened the resin in this region of interest. While the higher  
713 magnification image collected was free of artefacts, this can lead to a subsequent series of images  
714 where the sample underlying the region of interest appears distorted. This panel also illustrates  
715 the issue of debris accumulation on the block face (arrow) during imaging, also denoted by the  
716 arrow in panel E. If this becomes a persistent imaging problem, it will be necessary to break the  
717 vacuum, open the chamber and blow away debris accumulated on the diamond knife and around  
718 the sample. Small discharges of electrons from the block-face can lead to the rapid contrast  
719 changes and lines denoted by the white arrowhead. (C) This image illustrates knife scratches on  
720 the block face. This can occur due to a damaged knife, or debris accumulation on the edge of the  
721 knife. (D) The artefact denoted (arrow) is a result of the electron beam focused on (without  
722 sectioning) the block face for an extended period of time with the sample still in the imaging  
723 chamber. (E) Improper fixation of tissue can lead to separation of cellular structures and  
724 connective tissue (\*). (F) If a large amount of charging occurs in your tissue or resin block,  
725 subsequent accumulation and discharge can occur which leads to the image “skipping” as is seen  
726 in this image. Note the distortion of the tissue in the image at these skipping points (arrows).  
727 Panel A scale bar = 1  $\mu\text{m}$ . Panel B scale bar = 2  $\mu\text{m}$ . Panel C scale bar = 5  $\mu\text{m}$ . Panel D scale bar =  
728 2  $\mu\text{m}$ . Panel E scale bar = 25  $\mu\text{m}$ . Panel F scale bar = 50  $\mu\text{m}$ .

729

730 **Figure 11: Imaging tissue at 3 kV using various pixel dwell times and beam intensities.** All images  
731 were collecting using a 3 kV beam, beam intensity is on a device-specific scale ranging from 1 to  
732 20. The field imaged is of the vascular lumen containing white and red blood cells. At this low kV  
733 it is difficult to appreciate cellular detail. Increasing the pixel dwell time had little effect.  
734 Increasing beam intensity to 6 improved image contrast.

735

736 **Figure 12: Imaging tissue at 7 kV using various pixel dwell times and beam intensities.** All images  
737 were collected using a 7 kV beam, beam intensity is on a device-specific scale ranging from 1 to  
738 20. The field imaged is of the vascular lumen containing white and red blood cells. At 7 kV,  
739 increasing beam intensity and pixel dwell time contributed to higher quality imaging.

740

741 **Figure 13: Imaging tissue at 12 kV using various pixel dwell times and beam intensities.** All  
742 images were collected using a 12 kV beam, beam intensity is on a device-specific scale ranging  
743 from 1 to 20. The field imaged is of the vascular lumen containing white and red blood cells. At  
744 12 kV, imaging is optimized by adjusting pixel dwell time and beam intensity. Charging is  
745 reduced/absent at shorter pixel dwell times while cellular detail and image contrast are best with  
746 a longer pixel dwell time and higher beam intensity.

747

748 **DISCUSSION:**

749 The purpose of this methods paper is to highlight the tissue preparation and imaging  
750 methodology that has allowed our lab to reliably capture high-resolution serial electron  
751 microscopy images, and to point out critical steps that lead to this outcome as well as potential  
752 pitfalls that can occur when conducting SBF-SEM imaging. Success using this protocol requires  
753 proper fixation of tissue, impregnation of heavy metals into the sample, modifications of the  
754 embedding resin to reduce charging, as well as an understanding of the microscope and imaging  
755 settings used to collect images. The maxim, “quality in, quality out” is an appropriate axiom for  
756 SBF-SEM imaging. As the goal of SBF-SEM often is the appreciation or quantification of  
757 ultrastructural detail, extra care must be given to fixation strategy in order to ensure that tissue  
758 distortion does not occur. If tissue becomes distorted at any point in the preparation of samples  
759 (i.e., undergoes swelling, shrinking, or disruption of cellular morphology), then tissue  
760 reconstruction and quantization will not yield accurate data. Furthermore, the use of incorrect  
761 imaging settings can lead to loss of data that cannot be recaptured as SBF-SEM imaging is a  
762 destructive process. Additionally, care must be used when loading a tissue sample as the delicate  
763 diamond knife can be damaged by hasty or incorrect sample preparation. This can result in chips  
764 or breaks in the knife, which can leave visible scratch marks in images (**Figure 10C**). The diamond  
765 knife can also be damaged by calcified structures, hard granules, or accidentally embedded glass  
766 (e.g., from reagent ampules).

767  
768 While the majority of SBF-SEM literature to date uses beam acceleration voltages in the range of  
769 1 to 3 kV alongside pixel dwell times closer to 1-5  $\mu\text{s}/\text{px}$  (**Figure 11**)<sup>45-49</sup>, the current protocol uses  
770 acceleration voltages of 7-12 kV and a pixel dwell time of 12  $\mu\text{s}/\text{px}$  for serial imaging and 32  $\mu\text{s}/\text{px}$   
771 for imaging regions of interest (**Figures 12 & 13**). These settings, coupled with a slice thickness of  
772 100-200 nm allows for high-quality and high resolution imaging of a wide range of biological  
773 tissue. Increased acceleration voltage allows for an increase in contrast, resolution, as well as  
774 signal-to-noise ratio. Increased dwell time further increases resolution and signal-to-noise ratio,  
775 while increased slice thickness leads to decreased charging on the block surface during sectioning  
776 and combats beam-induced damage in subsequent images<sup>14</sup>. While this imaging method may  
777 differ from convention, the images and datasets produced speak for themselves. If we had to  
778 speculate on the reason for this success, it is possible that it is a result of our unique combination  
779 of high kV values, longer pixel dwell times, and block preparation. Increasing imaging kV results  
780 in an increased interaction volume between the electron beam and the sample. This interaction  
781 volume is both deeper as well as wider resulting in a theoretical increase in the number of  
782 electrons detected that originate from deeper within the sample block, or from a wider cross  
783 section of tissue as the spot size teardrop increases in diameter. As SBF-SEM is interested in the  
784 surface detail of the block, this results in a theoretical decrease in signal-to-noise ratio. However,  
785 the increase in kV also pushes electrons deeper into the sample where they are less likely to  
786 escape the block and contribute to the electrons collected by the detector. With the added  
787 benefit of an increased signal via longer pixel dwell times and higher beam intensity, it is possible  
788 that this imaging method results in a greater increase in signal from the sample surface in relation  
789 to noise originating within the interaction volume. Additionally, the increased sample  
790 conductivity introduced with carbon black as well as silver and gold coating helps to ameliorate  
791 charge buildup which now occurs deeper within the block and further from the block-face.  
792 Indeed, **Figures 11-13** show that as kV is increased sample charging begins to diminish as it is

793 potentially pushed deeper into the block. Samples imaged at low magnification can be captured  
794 with adequate contrast using the conventional settings, however these images often lack detail  
795 upon close inspection. Our data clearly show that when using relatively high magnification where  
796 the goal is cellular detail, increasing the conventional settings can produce exceptional results.  
797 The 2020 article by P. Goggin, et al provides a useful table outlining the effect of changing imaging  
798 settings on final image quality, and is a helpful reference to consult if optimizing the protocol for  
799 novel tissues becomes necessary<sup>14</sup>. The 100-200 nm slice thickness recommended in this protocol  
800 has the added benefit of allowing the collection of large SBF-SEM data sets at a rapid rate. While  
801 collecting images at 12 $\mu$ s/px for example, imaging through a 100  $\mu$ m depth at 2048x2048 px  
802 requires ~14 hours while sectioning at 100nm/section but would require ~56 hours if sectioned  
803 at 25nm/section. While x,y resolution remains unchanged as a result of section thickness, not  
804 accounting for the added ability to image using higher kV values and pixel dwell times that come  
805 with larger sections, it is important to note that the resolution along the z-axis does suffer. The  
806 loss of z-resolution is an important consideration and should be contemplated when deciding  
807 how tissue should be oriented in the resin block and in relation to the imaging plane, and has the  
808 potential to preclude the study of smaller cell features or interactions (e.g., synaptic invaginations  
809 or intracellular features on the scale of tens of nanometers). However, in addition to rapid  
810 imaging time, this protocol has additional added benefits in that it rapidly produces ideal datasets  
811 for stereological analysis as well as the study of rare biological events or cells. Larger section  
812 thickness can also aid in manual 3D reconstruction, as a 100  $\mu$ m region sectioned at 100  
813 nm/section would require manual segmentation of 1,000 images while the same region  
814 sectioned at 25 nm/section would require manual segmentation of 4,000 images.

815  
816 SBF-SEM has the benefit of generating large datasets in a relatively short period. While data  
817 analysis can be performed using quantitative methods such as stereology, which will be discussed  
818 below, it can often be informative to create 3D reconstructions via image segmentation. An  
819 image stack created using SBF-SEM can be thought of as a collection of voxels, while  
820 segmentation is the process of assigning these voxels to user-defined objects thereby creating  
821 3D representations of tissue structures. These reconstructions often provide a heretofore unseen  
822 perspective on tissue ultrastructure and cell-cell interaction (**Figures 5-9**). Furthermore, once  
823 reconstructions have been created it is possible to use data inherent in the reconstructions to  
824 extract a wealth of information from segmented tissue. Parameters ranging from surface area,  
825 volume, length and distance, as well as angular data are all readily available once a reconstruction  
826 has been created<sup>50,51</sup>. While this can be incredibly useful, especially when paired with videos and  
827 images pulled from reconstructed data sets, the time required for manual segmentation is an  
828 important consideration when attempting to extrapolate data from SBF-SEM datasets. There are  
829 currently a host of both free and purchasable software available for the manual and semi-manual  
830 segmentation of SBF-SEM image stacks. One free option for reconstruction software is the image  
831 processing package Fiji for ImageJ, an open source image processing program, which contains a  
832 segmentation editor plugin that allows for manual segmentation<sup>52,53</sup>. Additionally, the software  
833 Reconstruct offers an alternative free segmentation option<sup>54</sup> (**Figure 8**). While potentially  
834 expensive, purchasable options often contain more robust feature sets, such as semi-automated  
835 segmentation processes or movie and image creation suites. One such option was used to create  
836 the reconstructions found in **Figures 5-7 and 9** (Details available in **Table of Materials**).

837 Additionally, tools are available for the creation, analysis, and rendering of contrast-based 3D  
838 reconstructions using virtual reality with the potential to greatly speed up the reconstruction  
839 process<sup>20,55</sup>. While not always available for all applications, a host of software tools are available  
840 for computer assisted manual segmentation which have the potential to greatly decrease the  
841 time required for segmentation<sup>56-58</sup>. Regardless of the software used, considerable forethought  
842 and an understanding of the question being answered, or gap in knowledge to be filled, by serial  
843 reconstructions should precede segmentation, as the process is laborious and time-intensive.

844  
845 The production of 3D reconstructions comes with its own considerations. With larger data sets  
846 processing power can be a limiting factor, and so optimizing the use of system resources can be  
847 critical for maintaining a productive workflow and speeding up the reconstruction and rendering  
848 process. When rendering a 3D reconstruction, most software converts segmented image stacks  
849 into a surface comprised of interconnected triangles. If a reconstruction project is large or  
850 intricate, the rendering of these triangles can require a great deal of computing power. While  
851 working on a 3D reconstruction, it can be helpful to limit the number of triangles the  
852 reconstruction software can use to convert the segmented images into reconstructed surfaces.  
853 This can be useful for monitoring the progress of a 3D reconstruction during the segmentation  
854 process. Once segmentation is complete, the triangle limit can be removed before rendering  
855 images or videos of reconstructions. Alternatively, and if the reconstruction software allows for  
856 it, we have found success monitoring the progress of a reconstruction using volume rendering  
857 rather than surface generation. Volume rendering, while not as suitable for images or videos  
858 meant for publication or presentation, requires far less processing power and as such can be  
859 helpful in providing a smooth experience when reconstructing and preparing images and videos  
860 of reconstructions. Additionally, it is best practice when manually segmenting an SBF-SEM data  
861 set to define every object to be reconstructed with its own unique identifier. If a field of epithelial  
862 cells is being reconstructed for example, rather than assigning all epithelial cells to a voxel group  
863 entitled “epithelium,” each epithelial cell should be assigned its own moniker (i.e., Epi1, Epi2,  
864 Epi3, etc.). This affords greater freedom when the reconstruction is complete, as each cell can be  
865 either included or excluded from the final rendering, assigned different colors or transparencies,  
866 or removed or introduced individually if a video is being produced. Furthermore, this allows  
867 metrics such as surface area or volume to be collected from each reconstructed object rather  
868 than the object group as a whole.

869  
870 Another incredibly powerful tool for extracting quantitative data from SBF-SEM image stacks is  
871 the practice of stereology. Stereology takes advantage the inherent mathematical relationships  
872 between three-dimensional objects and their two-dimensional representations (i.e., electron  
873 micrographs). SBF-SEM data sets are ideal for the application of stereology, as this method for  
874 extracting 3D information from large datasets is considerably less time- and labor-intensive when  
875 compared to segmented reconstruction. Stereology generally consists of applying geometric  
876 grids to random, uniformly sampled images and has been used extensively over the past 50 years  
877 in order to produce accurate and unbiased estimates of cell/organelle number, length, surface  
878 area, and volume<sup>21,59-63</sup>. While 3D reconstructions can be impressive and provide a novel  
879 perspective on biological tissues, it is often quicker, more accurate, reproducible, and conducive  
880 for large sample sizes to use a stereological approach to data extraction. While there are many

881 papers discussing the practical application of stereology<sup>64-66</sup>, a number of textbooks provide  
882 useful, in-depth overviews of the methodology as well as provide a number of stereological grids  
883 which can be applied to the study of tissue ultrastructure<sup>67-69</sup>.

884  
885 SBF-SEM is a powerful imaging method that allows for the three-dimensional appreciation of  
886 tissue ultrastructure. While the ability to create 3D datasets with SEM resolution puts previously  
887 unanswerable questions within our reach, proper tissue preparation and an understanding of  
888 SBF-SEM imaging is paramount for the success of studies that utilize this microscopy method. It  
889 is our hope that the application of this protocol to future studies will lead to greater and greater  
890 insight into the biological mysteries that surround us, and continue to push us further into the  
891 frontiers of human knowledge.

892  
893 **ACKNOWLEDGMENTS:**

894 We would like to thank Dr. Sam Hanlon, Evelyn Brown, and Margaret Gondo for their excellent  
895 technical assistance. This research was supported in part by National Institutes of Health (NIH)  
896 R01 EY-018239 and P30 EY007551 (National Eye Institute), in part by the Lion's Foundation for  
897 Sight, and in part by NIH 1R15 HD084262-01 (National Institute of Child Health & Human  
898 Development).

899  
900 **DISCLOSURES:**

901 The authors have nothing to disclose.

902  
903 **REFERENCES:**

- 904  
905 1 Leighton, S. B. SEM images of block faces, cut by a miniature microtome within the SEM -  
906 a technical note. *Scanning Electron Microscopy*. (Pt 2), 73-76 (1981).  
907 2 Denk, W., Horstmann, H. Serial block-face scanning electron microscopy to reconstruct  
908 three-dimensional tissue nanostructure. *PLOS Biology*. **2** (11), e329 (2004).  
909 3 He, Q., Hsueh, M., Zhang, G., Joy, D. C., Leapman, R. D. Biological serial block face scanning  
910 electron microscopy at improved z-resolution based on Monte Carlo model. *Scientific Reports*. **8**  
911 (1), 12985 (2018).  
912 4 Zankel, A., Wagner, J., Poelt, P. Serial sectioning methods for 3D investigations in  
913 materials science. *Micron*. **62**, 66-78 (2014).  
914 5 Titze, B., Genoud, C. Volume scanning electron microscopy for imaging biological  
915 ultrastructure. *Biology of the Cell*. **108** (11), 307-323 (2016).  
916 6 Ohta, K. et al. Beam deceleration for block-face scanning electron microscopy of  
917 embedded biological tissue. *Micron*. **43** (5), 612-620 (2012).  
918 7 Bouwer, J. C. et al. Deceleration of probe beam by stage bias potential improves  
919 resolution of serial block-face scanning electron microscopic images. *Advanced Structural and*  
920 *Chemical Imaging*. **2** (1), 11 (2017).  
921 8 Kizilyaprak, C., Longo, G., Daraspe, J., Humbel, B. M. Investigation of resins suitable for  
922 the preparation of biological sample for 3-D electron microscopy. *Journal of Structural Biology*.  
923 **189** (2), 135-146 (2015).  
924 9 Kittelmann, M., Hawes, C., Hughes, L. Serial block face scanning electron microscopy and

925 the reconstruction of plant cell membrane systems. *Journal of Microscopy*. **263** (2), 200-211  
926 (2016).

927 10 Biazik, J., Vihinen, H., Anwar, T., Jokitalo, E., Eskelinen, E. L. The versatile electron  
928 microscope: an ultrastructural overview of autophagy. *Methods*. **75**, 44-53 (2015).

929 11 Peddie, C. J., Collinson, L. M. Exploring the third dimension: Volume electron microscopy  
930 comes of age. *Micron*. **61**, 9-19 (2014).

931 12 Piños, J., Mikmeková, Š., Frank, L. About the information depth of backscattered electron  
932 imaging. *Journal of Microscopy*. **266** (3), 335-342 (2017).

933 13 Smith, D., Starborg, T. Serial block face scanning electron microscopy in cell biology:  
934 Applications and technology. *Tissue Cell*. **57**, 111-122 (2019).

935 14 Goggin, P. et al. Development of protocols for the first serial block-face scanning electron  
936 microscopy (SBF SEM) studies of bone tissue. *Bone*. **131**, 115107 (2020).

937 15 Deerinck, T. J. et al. High-performance serial block-face SEM of nonconductive biological  
938 samples enabled by focal gas injection-based charge compensation. *Journal of Microscopy*. **270**  
939 (2), 142-149 (2018).

940 16 Nguyen, H. B. et al. Conductive resins improve charging and resolution of acquired images  
941 in electron microscopic volume imaging. *Scientific Reports*. **6**, 23721 (2016).

942 17 Deerinck, T. J., Bushong, E. A., Thor, A., Ellisman, M. H. NCMIR methods for 3D EM: a new  
943 protocol for preparation of biological specimens for serial block face scanning electron  
944 microscopy. *National Center for Microscopy and Imaging Research*. **6** (8) (2010).

945 18 Deerinck, T. J. et al. Enhancing Serial Block-Face Scanning Electron Microscopy to Enable  
946 High Resolution 3-D Nanohistology of Cells and Tissues. *Microscopy and Microanalysis*. **16** (S2),  
947 1138-1139 (2010).

948 19 Kubota, Y. New developments in electron microscopy for serial image acquisition of  
949 neuronal profiles. *Microscopy (Oxf)*. **64** (1), 27-36 (2015).

950 20 Courson, J. A. et al. Serial block-face scanning electron microscopy: A provocative  
951 technique to define 3-dimensional ultrastructure of microvascular thrombosis. *Thrombosis*  
952 *Research*. **196**, 519-522 (2020).

953 21 Courson, J. A. et al. Serial block-face scanning electron microscopy reveals neuronal-  
954 epithelial cell fusion in the mouse cornea. *PLoS One*. **14** (11), e0224434 (2019).

955 22 Lafontant, P. J. et al. Cardiac Myocyte Diversity and a Fibroblast Network in the Junctional  
956 Region of the Zebrafish Heart Revealed by Transmission and Serial Block-Face Scanning Electron  
957 Microscopy. *PLoS One*. **8** (8), e72388 (2013).

958 23 Hanlon, S. D., Behzad, A. R., Sakai, L. Y., Burns, A. R. Corneal stroma microfibrils.  
959 *Experimental Eye Research*. **132**, 198-207 (2015).

960 24 Gage, G. J., Kipke, D. R., Shain, W. Whole animal perfusion fixation for rodents. *Journal of*  
961 *Visualized Experiments*. 10.3791/3564 (65) (2012).

962 25 Davenport, A. T., Grant, K. A., Szeliga, K. T., Friedman, D. P., Daunais, J. B. Standardized  
963 method for the harvest of nonhuman primate tissue optimized for multiple modes of analyses.  
964 *Cell Tissue Bank*. **15** (1), 99-110 (2014).

965 26 Schuster, A. et al. An isolated perfused pig heart model for the development, validation  
966 and translation of novel cardiovascular magnetic resonance techniques. *Journal of*  
967 *Cardiovascular Magnetic Resonance*. **12** (1), 53 (2010).

968 27 Hanlon, S. D., Patel, N. B., Burns, A. R. Assessment of postnatal corneal development in

969 the C57BL/6 mouse using spectral domain optical coherence tomography and microwave-  
970 assisted histology. *Experimental Eye Research*. **93** (4), 363-370 (2011).

971 28 Longi eras, N., Sebban, M., Palmas, P., Rivaton, A., Gardette, J. L. Multiscale approach to  
972 investigate the radiochemical degradation of epoxy resins under high-energy electron-beam  
973 irradiation. *Journal of Polymer Science Part A: Polymer Chemistry*. **44** (2), 865-887 (2006).

974 29 Hashimoto, T., Thompson, G. E., Zhou, X., Withers, P. J. 3D imaging by serial block face  
975 scanning electron microscopy for materials science using ultramicrotomy. *Ultramicroscopy*. **163**,  
976 6-18 (2016).

977 30 Rouquette, J. et al. Revealing the high-resolution three-dimensional network of chromatin  
978 and interchromatin space: A novel electron-microscopic approach to reconstructing nuclear  
979 architecture. *Chromosome Research*. **17** (6), 801 (2009).

980 31 Briggman, K. L., Helmstaedter, M., Denk, W. Wiring specificity in the direction-selectivity  
981 circuit of the retina. *Nature*. **471** (7337), 183-188 (2011).

982 32 Katoh, K. Microwave-Assisted Tissue Preparation for Rapid Fixation, Decalcification,  
983 Antigen Retrieval, Cryosectioning, and Immunostaining. *International Journal of Biochemistry &*  
984 *Cell Biology*. **2016**, 7076910 (2016).

985 33 Login, G. R., Dvorak, A. M. A review of rapid microwave fixation technology: its expanding  
986 niche in morphologic studies. *Scanning*. **15** (2), 58-66 (1993).

987 34 Jamur, M. C., Faraco, C. D., Lunardi, L. O., Siraganian, R. P., Oliver, C. Microwave fixation  
988 improves antigenicity of glutaraldehyde-sensitive antigens while preserving ultrastructural  
989 detail. *Journal of Histochemistry and Cytochemistry*. **43** (3), 307-311 (1995).

990 35 Leong, A. S., Sormunen, R. T. Microwave procedures for electron microscopy and resin-  
991 embedded sections. *Micron*. **29** (5), 397-409 (1998).

992 36 Willingham, M. C., Rutherford, A. V. The use of osmium-thiocarbohydrazide-osmium  
993 (OTO) and ferrocyanide-reduced osmium methods to enhance membrane contrast and  
994 preservation in cultured cells. *Journal of Histochemistry and Cytochemistry*. **32** (4), 455-460  
995 (1984).

996 37 Khan, A. A., Riemersma, J. C., Booij, H. L. The reactions of osmium tetroxide with lipids  
997 and other compounds. *Journal of Histochemistry and Cytochemistry*. **9**, 560-563 (1961).

998 38 Belazi, D., Sol -Dom nech, S., Johansson, B., Schalling, M., Sj vall, P. Chemical analysis of  
999 osmium tetroxide staining in adipose tissue using imaging ToF-SIMS. *Histochemistry and Cell*  
1000 *Biology*. **132** (1), 105-115 (2009).

1001 39 Rivlin, P. K., Raymond, P. A. Use of osmium tetroxide-potassium ferricyanide in  
1002 reconstructing cells from serial ultrathin sections. *Journal of Neuroscience Methods*. **20** (1), 23-  
1003 33 (1987).

1004 40 Aguas, A. P. The use of osmium tetroxide-potassium ferrocyanide as an extracellular  
1005 tracer in electron microscopy. *Stain Technology*. **57** (2), 69-73 (1982).

1006 41 Seligman, A. M., Wasserkrug, H. L., Hanker, J. S. A new staining method (OTO) for  
1007 enhancing contrast of lipid-containing membranes and droplets in osmium tetroxide-fixed  
1008 tissue with osmiophilic thiocarbohydrazide(TCH). *Journal of Cell Biology*. **30** (2), 424-432 (1966).

1009 42 Watson, M. L. Staining of tissue sections for electron microscopy with heavy metals. II.  
1010 Application of solutions containing lead and barium. *Journal of Biophysical and Biochemical*  
1011 *Cytology*. **4** (6), 727-730 (1958).

1012 43 Zhou, W., Apkarian, R., Wang, Z., Joy, D. Fundamentals of Scanning Electron Microscopy.

1013 *Scanning Microscopy in Nanotechnology*. 1-40 (2006).

1014 44 Tapia, J. C. et al. High-contrast en bloc staining of neuronal tissue for field emission  
1015 scanning electron microscopy. *Nature Protocols*. **7** (2), 193-206 (2012).

1016 45 Buchacker, T. et al. Assessment of the Alveolar Capillary Network in the Postnatal Mouse  
1017 Lung in 3D Using Serial Block-Face Scanning Electron Microscopy. *Frontiers in Physiology*. **10**,  
1018 1357 (2019).

1019 46 Keeling, E. et al. 3D-Reconstructed Retinal Pigment Epithelial Cells Provide Insights into  
1020 the Anatomy of the Outer Retina. *International Journal of Molecular Sciences*. **21** (21) (2020).

1021 47 Shang, P. et al. Chronic Alcohol Exposure Induces Aberrant Mitochondrial Morphology  
1022 and Inhibits Respiratory Capacity in the Medial Prefrontal Cortex of Mice. *Frontiers in*  
1023 *Neuroscience*. **14**, 561173 (2020).

1024 48 Pfeifer, C. R. et al. Quantitative analysis of mouse pancreatic islet architecture by serial  
1025 block-face SEM. *Journal of Structural Biology*. **189** (1), 44-52 (2015).

1026 49 Wilke, S. A. et al. Deconstructing complexity: serial block-face electron microscopic  
1027 analysis of the hippocampal mossy fiber synapse. *Journal of Neuroscience*. **33** (2), 507-522 (2013).

1028 50 Cocks, E., Taggart, M., Rind, F. C., White, K. A guide to analysis and reconstruction of serial  
1029 block face scanning electron microscopy data. *Journal of Microscopy*. **270** (2), 217-234 (2018).

1030 51 Borrett, S., Hughes, L. Reporting methods for processing and analysis of data from serial  
1031 block face scanning electron microscopy. *Journal of Microscopy*. **263** (1), 3-9 (2016).

1032 52 Schindelin, J. et al. Fiji: an open-source platform for biological-image analysis. *Nature*  
1033 *Methods*. **9** (7), 676-682 (2012).

1034 53 Rueden, C. T. et al. ImageJ2: ImageJ for the next generation of scientific image data. *BMC*  
1035 *Bioinformatics*. **18** (1), 529 (2017).

1036 54 Fiala, J. C. Reconstruct: a free editor for serial section microscopy. *Journal of Microscopy*.  
1037 **218** (Pt 1), 52-61 (2005).

1038 55 Pidhorskyi, S., Morehead, M., Jones, Q., Spirou, G., Doretto, G. syGlass: interactive  
1039 exploration of multidimensional images using virtual reality Head-mounted displays. *arXiv*  
1040 *preprint arXiv:1804.08197*. (2018).

1041 56 Cardona, A. et al. TrakEM2 software for neural circuit reconstruction. *PLoS One*. **7** (6),  
1042 e38011 (2012).

1043 57 Belevich, I., Joensuu, M., Kumar, D., Vihinen, H., Jokitalo, E. Microscopy Image Browser: A  
1044 Platform for Segmentation and Analysis of Multidimensional Datasets. *PLOS Biology*. **14** (1),  
1045 e1002340 (2016).

1046 58 Luengo, I. et al. SuRVoS: Super-Region Volume Segmentation workbench. *Journal of*  
1047 *Structural Biology*. **198** (1), 43-53 (2017).

1048 59 Anderson, H. R., Stitt, A. W., Gardiner, T. A., Archer, D. B. Estimation of the surface area  
1049 and volume of the retinal capillary basement membrane using the stereologic method of vertical  
1050 sections. *Analytical & Quantitative Cytology & Histology*. **16** (4), 253-260 (1994).

1051 60 Gibbons, C. H., Illigens, B. M., Wang, N., Freeman, R. Quantification of sweat gland  
1052 innervation: a clinical-pathologic correlation. *Neurology*. **72** (17), 1479-1486 (2009).

1053 61 Knust, J., Ochs, M., Gundersen, H. J., Nyengaard, J. R. Stereological estimates of alveolar  
1054 number and size and capillary length and surface area in mice lungs. *Anat Rec (Hoboken)*. **292** (1),  
1055 113-122 (2009).

1056 62 Mahon, G. J. et al. Chloroquine causes lysosomal dysfunction in neural retina and RPE:



1057 implications for retinopathy. *Current Eye Research*. **28** (4), 277-284 (2004).  
1058 63 Michel, R. P., Cruz-Orive, L. M. Application of the Cavalieri principle and vertical sections  
1059 method to lung: estimation of volume and pleural surface area. *Journal of Microscopy*. **150** (Pt  
1060 2), 117-136 (1988).  
1061 64 Weibel, E. R. Stereological methods in cell biology: where are we--where are we going?  
1062 *Journal of Histochemistry and Cytochemistry*. **29** (9), 1043-1052 (1981).  
1063 65 Schmitz, C., Hof, P. R. Design-based stereology in neuroscience. *Neuroscience*. **130** (4),  
1064 813-831 (2005).  
1065 66 Kristiansen, S. L., Nyengaard, J. R. Digital stereology in neuropathology. *Apmis*. **120** (4),  
1066 327-340 (2012).  
1067 67 Howard, C. V., Reed, M. G. *Unbiased Stereology*. 2nd edn, (Garland Science/BIOS Scientific  
1068 Publishers, 2005).  
1069 68 Reith, A., Mayhew, T. M. *Stereology and Morphometry in Electron Microscopy: Problems  
1070 and Solutions*. (Hemisphere Publishing Corporation, 1988).  
1071 69 Mouton, P. R. *Principles and practices of unbiased stereology: an introduction for  
1072 bioscientists*. (Johns Hopkins University Press, 2002).  
1073

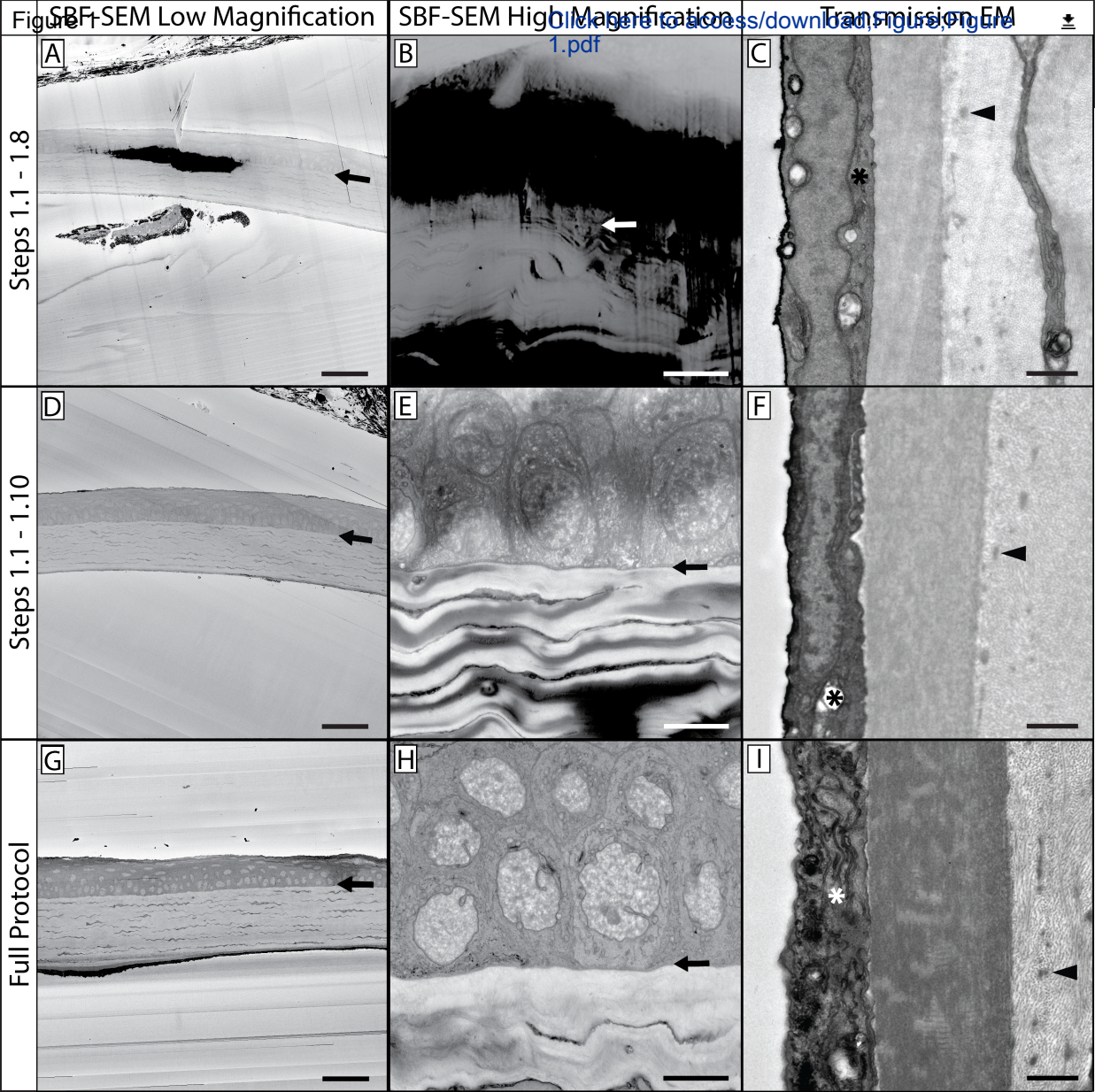
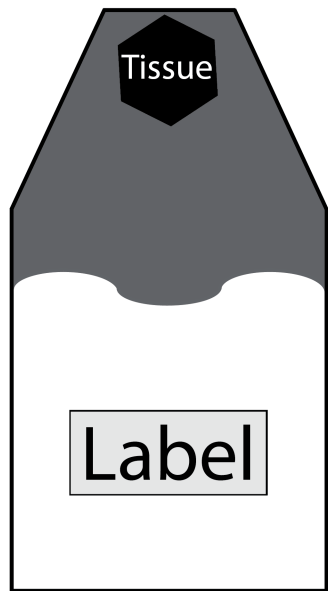
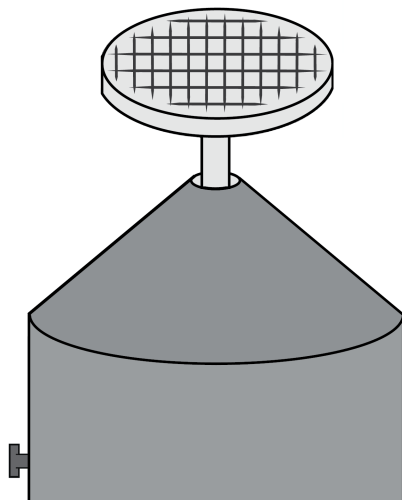


Figure 2

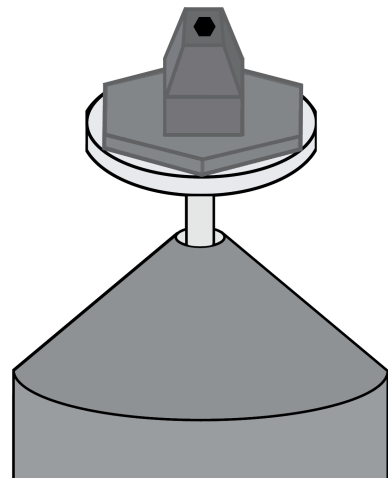


[Click here to access/download;Figure;Figure 2.pdf](#) 

**B**

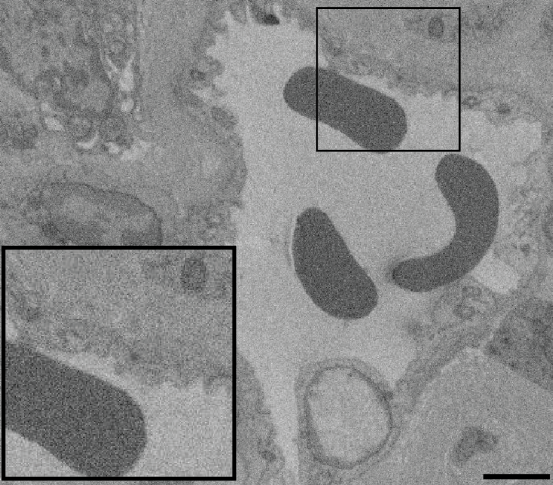


**C**

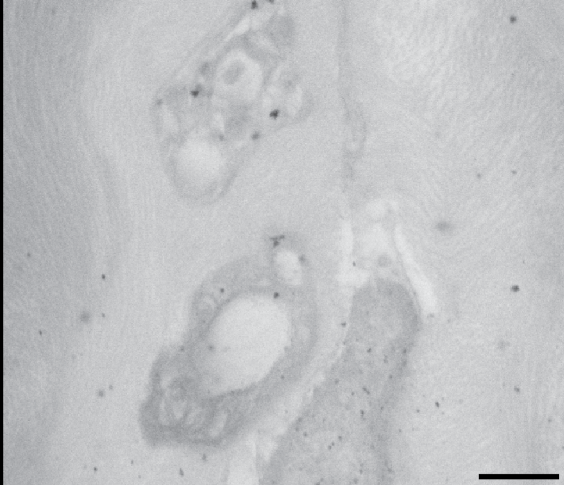




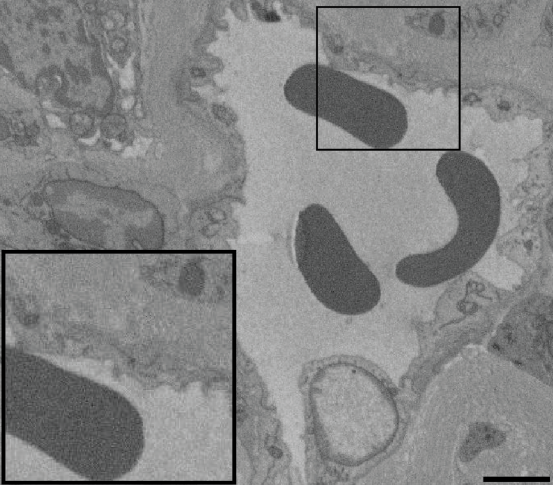
**A**



**C**



**B**



**D**

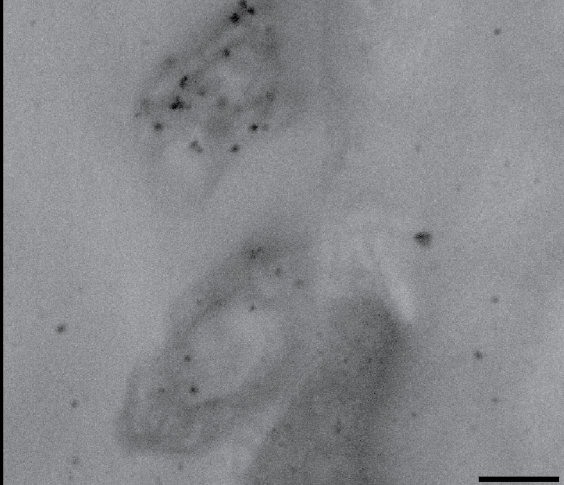
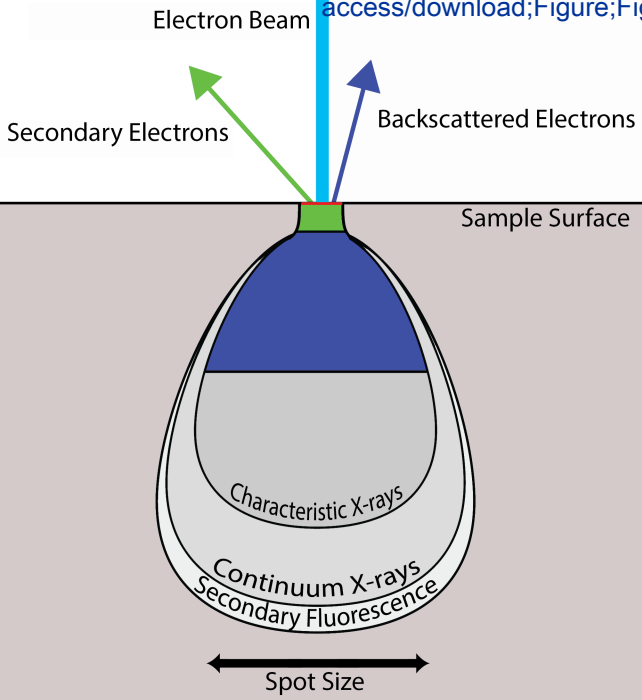
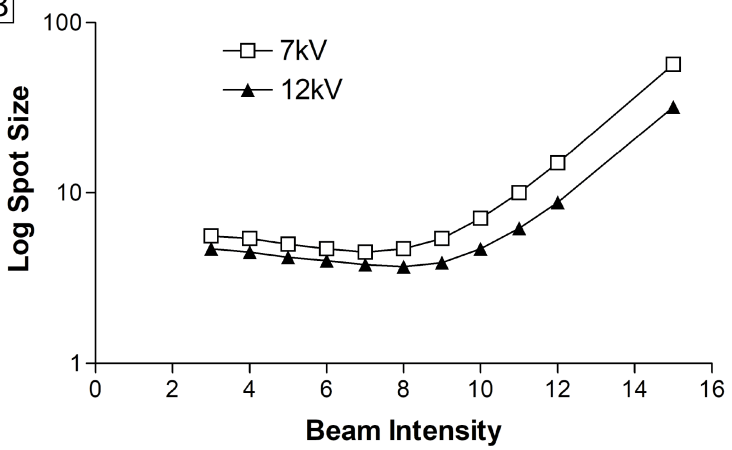


Figure 4

[Click here to access/download;Figure;Fig](#) 



B



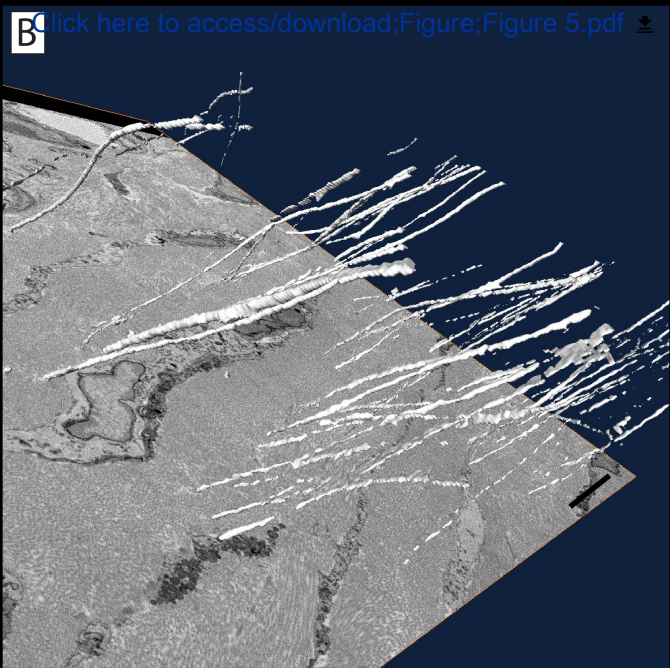
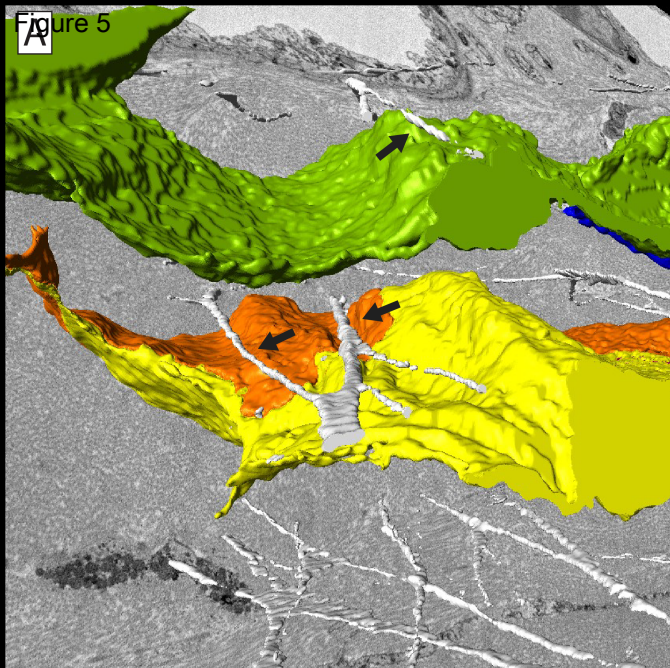
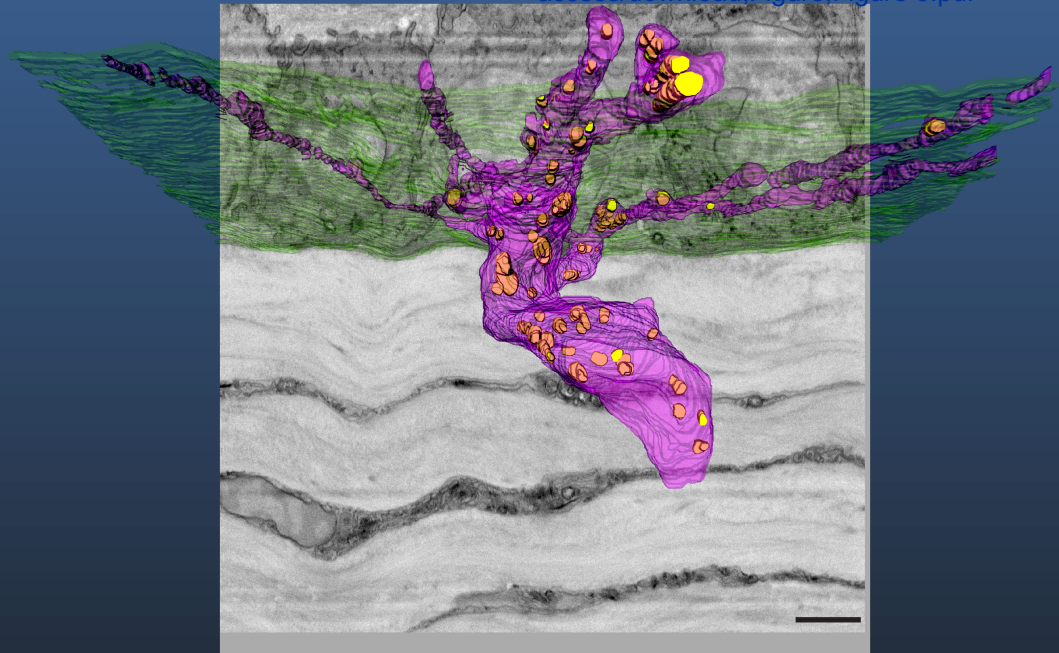
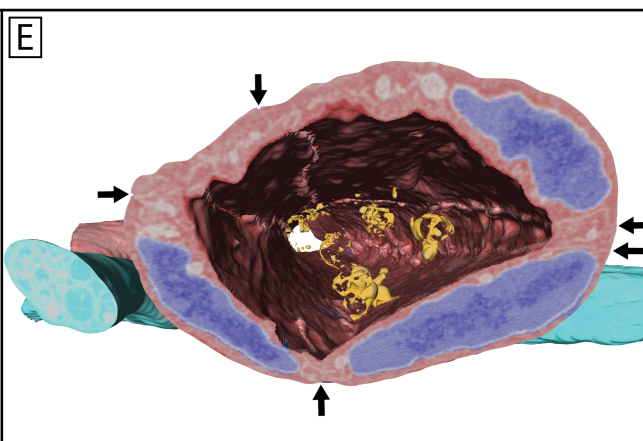
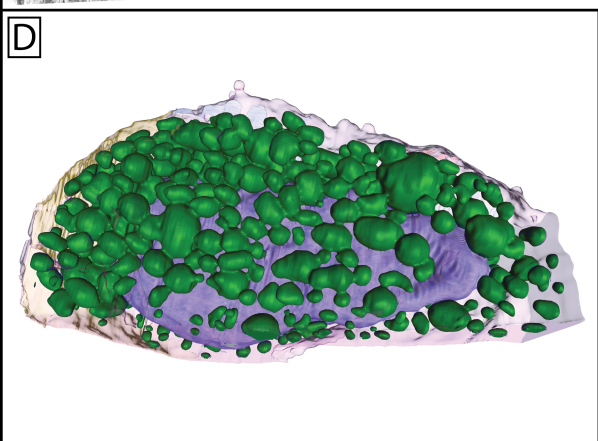
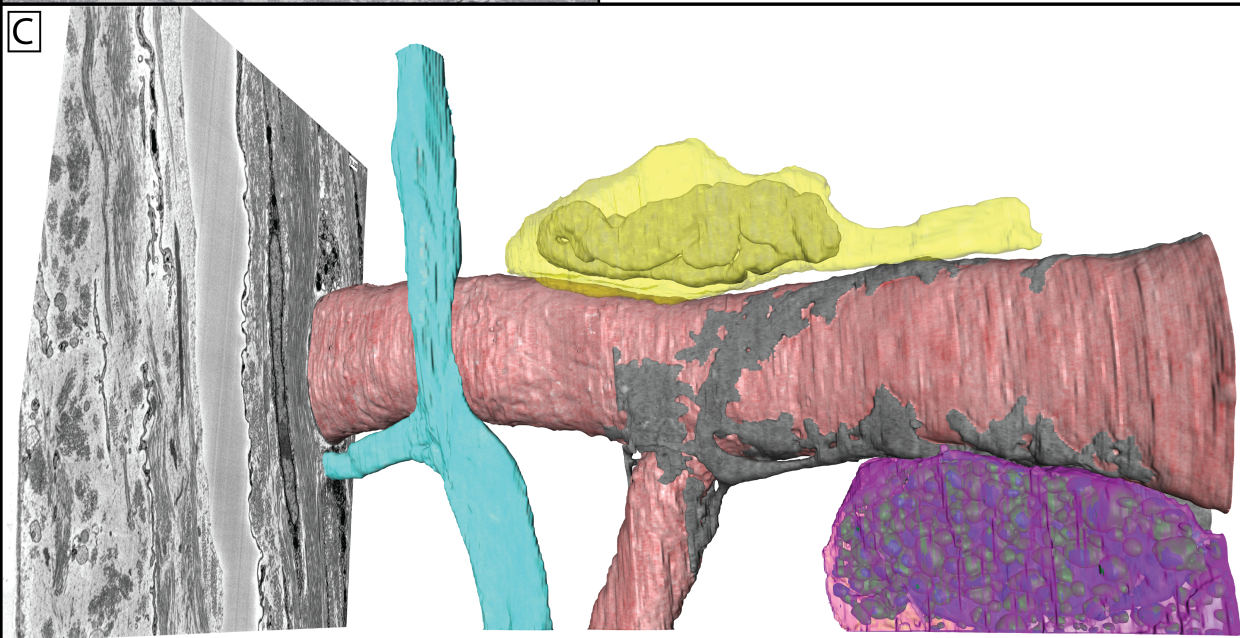
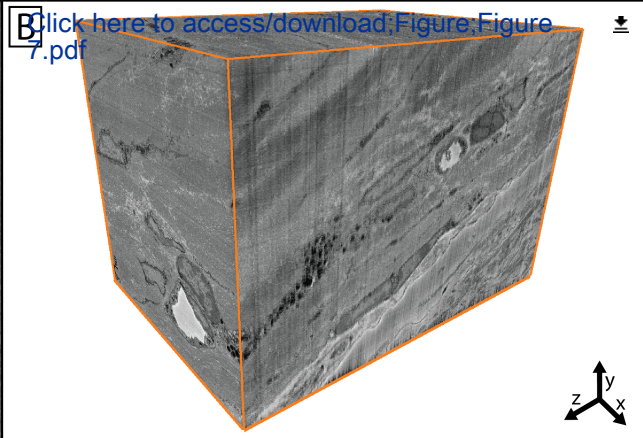
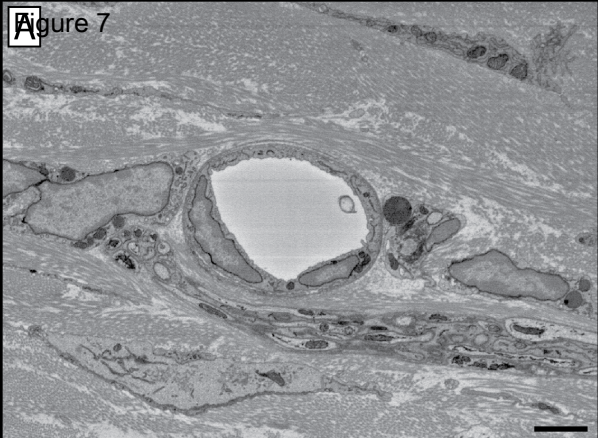




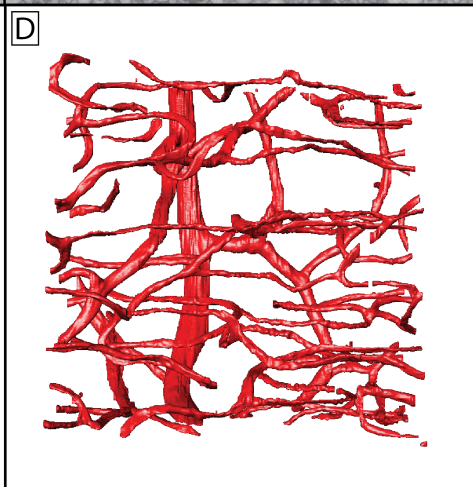
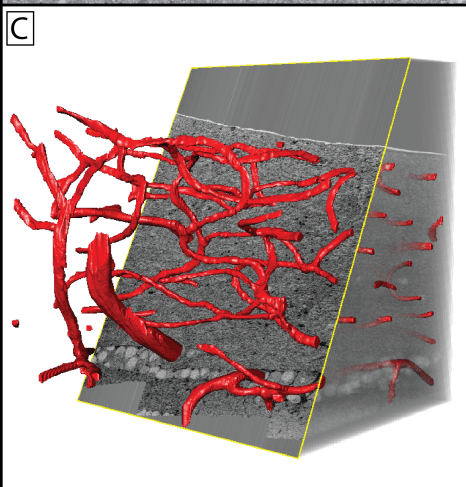
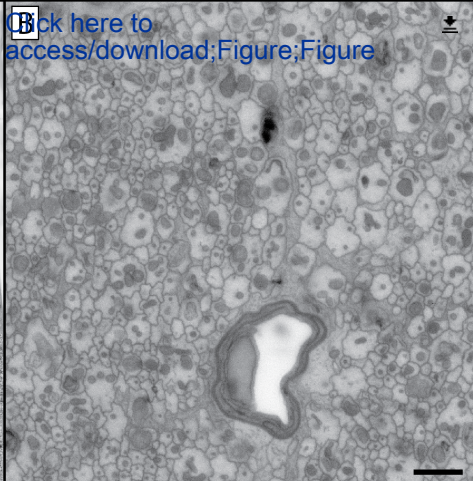
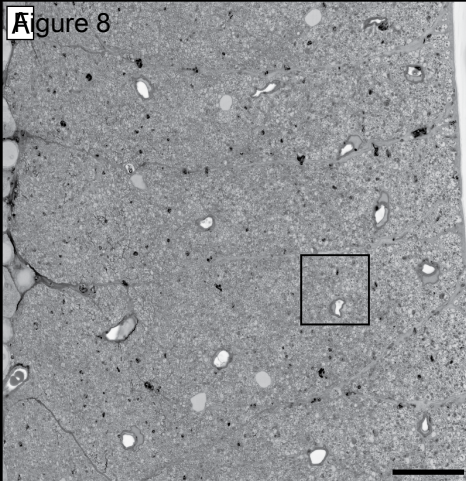
Figure 6

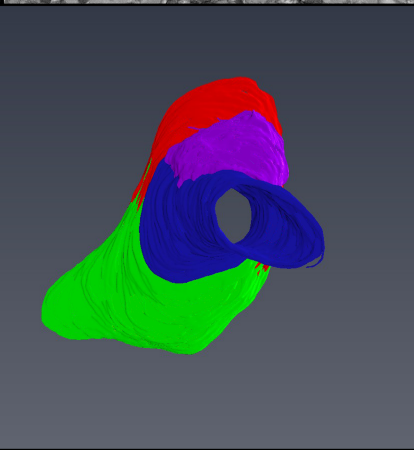
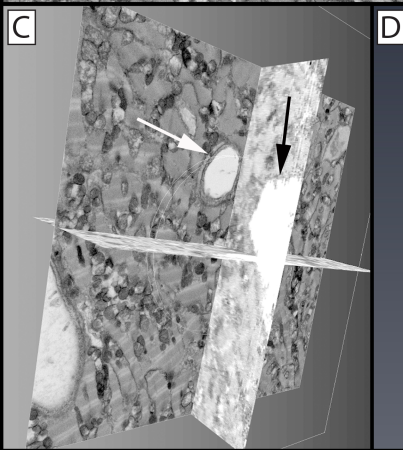
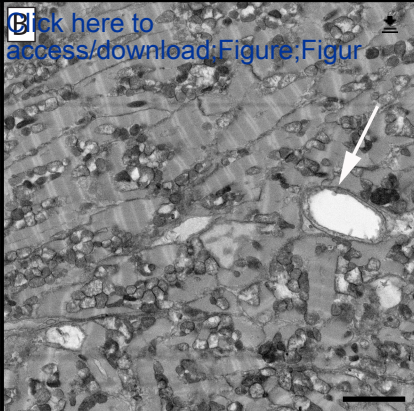
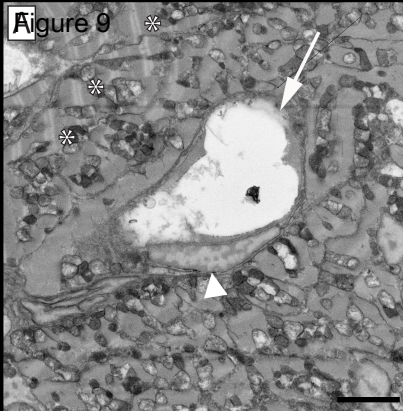
[Click here to access/download:Figure;Figure 6.pdf](#)



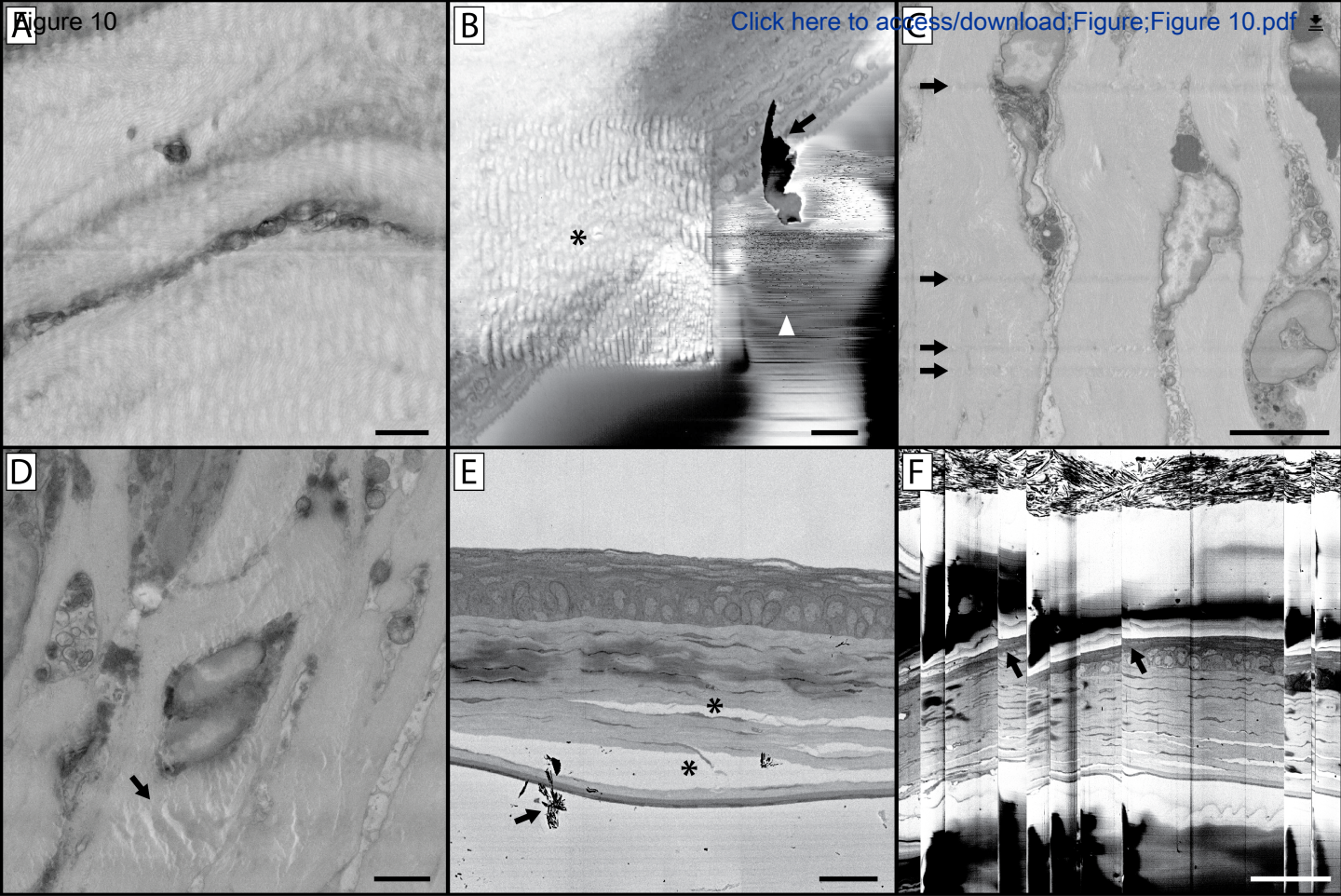












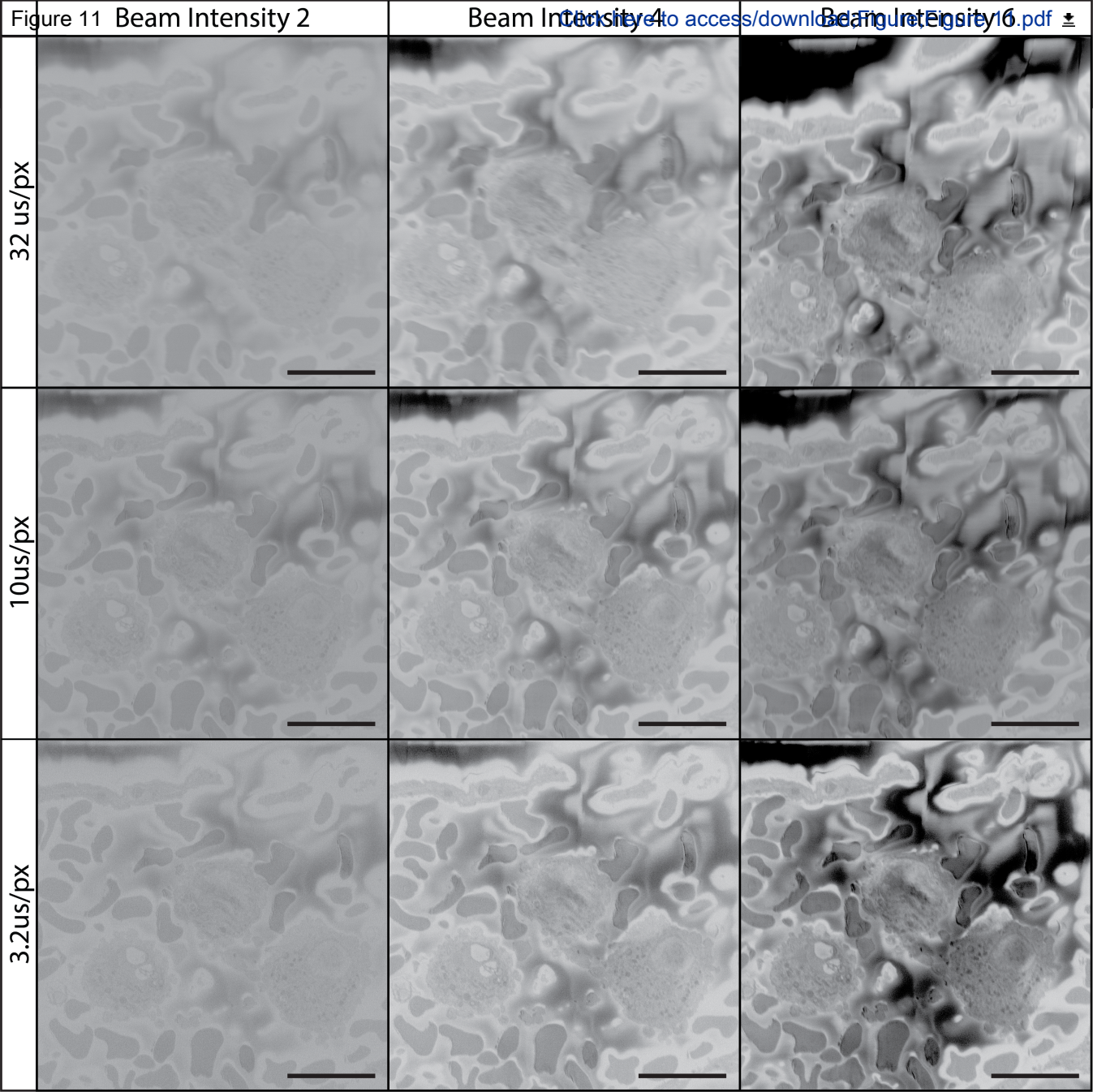
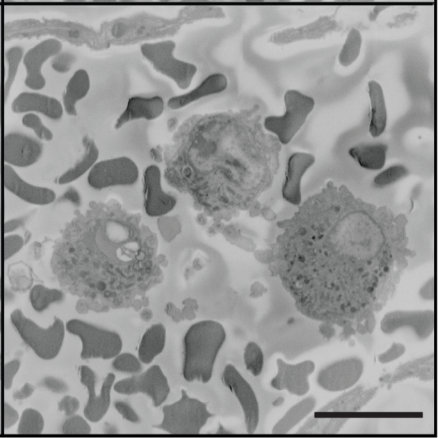
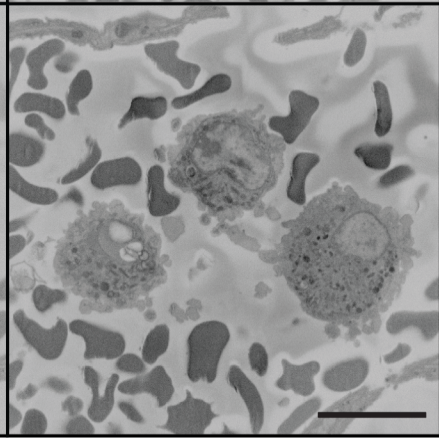
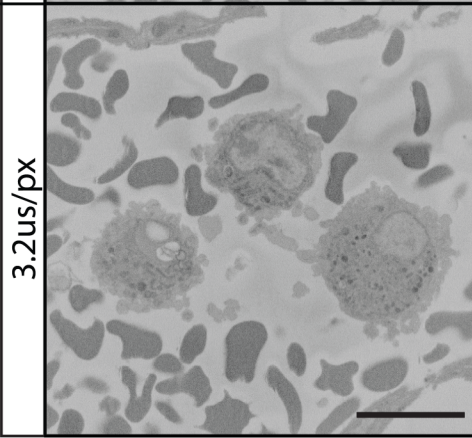
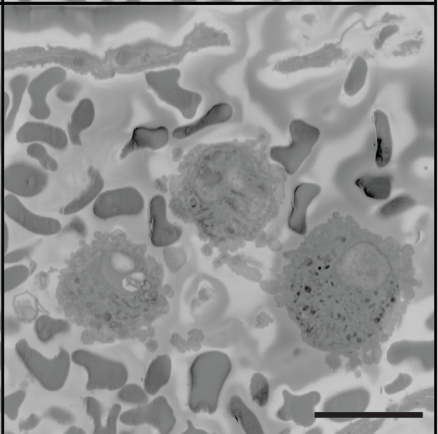
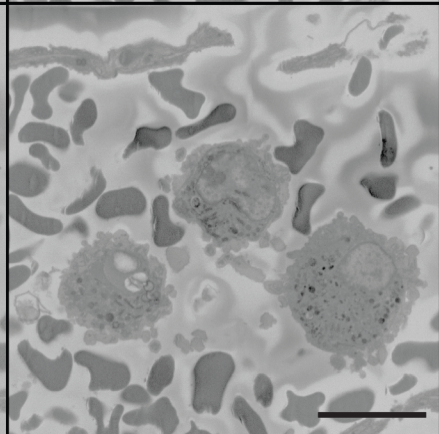
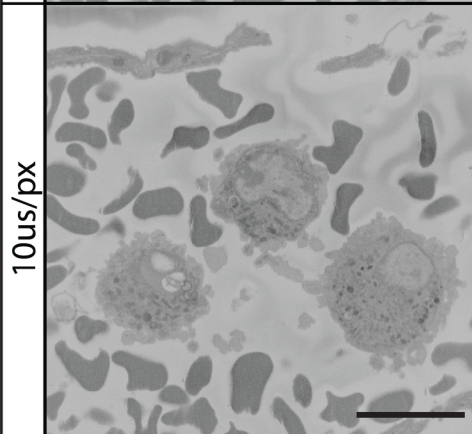
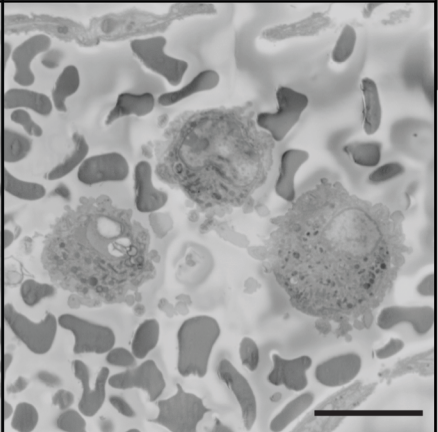
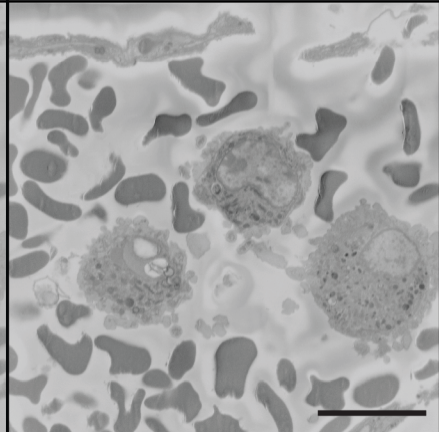
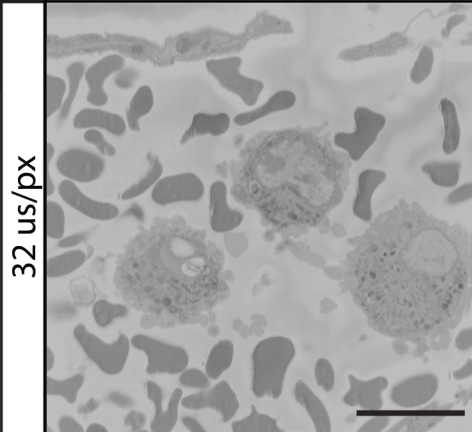




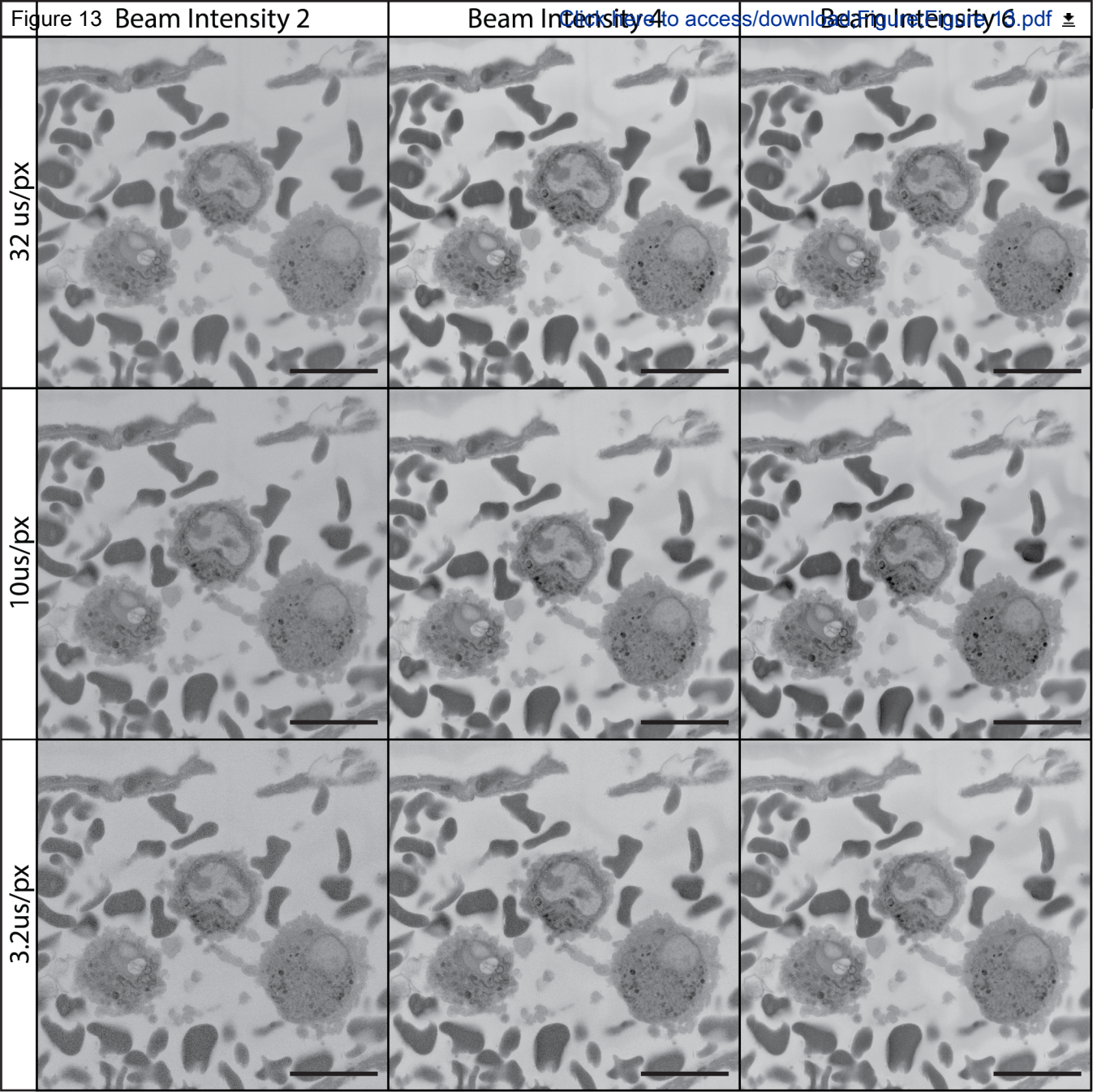
Figure 12 Beam Intensity 2

Beam Intensity 4

Beam Intensity 6







Name of Material/ Equipment
1/16 x 3/8 Aluminum Rivets
2.5mm Flathead Screwdriver
Acetone
Aspartic Acid
Calcium Chloride
Conductive Silver Paint
Denton Desk-II Vacuum Sputtering Device equipped with standard gold foil target
Double-edged Razors
Embed 812
Gatan 3View2 mounted in a Tescan Mira3 Field emission SEM
Glass Shell Vials, 0.5 DRAM (1.8 ml)
Gluteraldehyde
Gorilla Super Glue - Impact Tough
Ketjen Black
KOH
Lead Nitrate
Microwave
Osmium Tetroxide
Potassium Ferrocyanide
Silicone Embedding Mold
Sodium Cacodylate Trihydrate
Samco Transfer Pipette
Swiss Pattern Needle Files
Thiocarbohydrazide
Uranyl Acetate
Reconstruction Software
Amira Software
Fiji (Fiji is Just ImageJ)
Microscopy Image Browser (MIB)
Reconstuct Software
SuRVoS Workbench
SyGlass

Company	Catalog Number
Industrial Rivet & Fastener Co.	6N37RFLAP/1100
Wiha Quality Tools	27225
Electron Microscopy Sciences	RT 10000
Sigma-Aldrich	A8949
FisherScientific	C79-500
Ted Pella	16062
Denton Vacuum	N/A
Fisher Scientific	50-949-411
Electron Microscopy Sciences	14120
Gatan & Tescan	N/A
Electron Microscopy Sciences	72630-05
Electron Microscopy Sciences	16320
NA	NA
HM Royal	EC-600JD
FisherScientific	18-605-593
Fisher Scientific	L62-100
Pelco	BioWave Pro
Sigma-Aldrich	201030
Sigma-Aldrich	P9387
Ted Pella	10504
Electron Microscopy Sciences	12300
ThermoFisher Scientific	202
Electron Microscopy Sciences	62115
Sigma-Aldrich	223220
Polysciences, Inc.	21447-25

Thermo Scientific	N/A
ImageJ.net	N/A
University of Helsinki, Institute of Biotechnology	N/A
Neural Systems Lab	N/A
Diamond Light Source & The University of Nottingham	N/A
IstoVisio, Inc.	N/A



Notes

Used as specimen pins.

Used to dilute silver paint.

This is the gold-sputtering device used by the authors, alternates are acceptable.

This is the SBF-SEM device used by the authors, alternates are acceptable.

Referred to as cyanoacrylate glue in text.

Referred to as carbon black in text.

This is the microwave used by the authors, alternates are acceptable.

Used to make specimen pin storage tubes.

Used to create the reconstructions found in figures 5-7 and 9.

TrakEM2 can be added to Fiji to assist in manual segmentation.

Allows for reconstruction in virtual reality and histogram-based reconstruction methods.

*Please find below a point-by-point response to the reviewers' critiques and editorial comments. We would like to take this opportunity to thank the reviewers and editor for their constructive suggestions which we have incorporated into the manuscript, which we believe is now improved.*

**Editorial comments:**

Changes to be made by the Author(s):

1. Please take this opportunity to thoroughly proofread the manuscript to ensure that there are no spelling or grammar issues. Please define all abbreviations at first use.

*The manuscript has been proofread for spelling and grammar issues, and all abbreviations are defined at first use.*

2. Please make the title concise: Serial Block-Face Scanning Electron Microscopy (SBF-SEM) of Biological Tissue Samples.

*Thank you for this suggestion, the change has been made.*

3. Please specify the source of your tissue samples. In case you used animals and euthanized them to harvest tissue, please include an ethics statement before the numbered protocol steps, indicating that the protocol follows the guidelines of your institution's human research ethics committee.

*An ethics statement has been added to the manuscript prior to protocol steps.*

4. Please ensure that all text in the protocol section is written in the imperative tense as if telling someone how to do the technique (e.g., "Do this," "Ensure that," etc.). The actions should be described in the imperative tense in complete sentences wherever possible. Avoid usage of phrases such as "could be," "should be," and "would be" throughout the Protocol. Any text that cannot be written in the imperative tense may be added as a "Note." However, notes should be concise and used sparingly. Please include all safety procedures and use of hoods, etc. "Notes" should only be used to provide extraneous details, optional steps, or recommendations that are not critical to a step. Any text that provides details about how to perform a particular step should either be included in the step itself or added as a sub-step. Please consider moving some of the notes about the protocol to the discussion section.

*The protocol section has been proofread and changes made where necessary to maintain the imperative tense.*

5. JoVE cannot publish manuscripts containing commercial language. This includes trademark symbols (™), registered symbols (®), and company names before an instrument or reagent. Please remove all commercial language from your manuscript and use generic terms instead. All commercial products should be sufficiently referenced in the Table of Materials and Reagents.

For example: Ketjen Black, Denton Desk-II vacuum sputtering device, Reconstruct software, Amira Software (Thermo Scientific), spyglass software, etc

*All commercial language has been removed from the manuscript. Fiji/ImageJ and Reconstruct are both free, open-source NIH funded packages and as such were not removed but are properly cited as such.*

6. 1.1: To clarify the text, please revise to "Fix the tissue sample by immersing it in 0.1 M ...".

*We thank the editor for this suggestion, the change has been made to the manuscript text.*

7. Please include a scale bar for all images taken with a microscope to provide context to the magnification used. Define the scale in the appropriate Figure Legend.

*We thank the editor for this suggestion, the changes have been made to the manuscript figures and text.*

8. Discussion lines 673-675: instead of specifically citing these books, please state that stereology and its methodology have been described by various authors, and cite these books as reference.

*This change has been made to the manuscript text.*

9. Highlighting steps in the protocol indicates that you want to include those steps in the video and hence, will be used to prepare the script for filming the video. Please remove the highlighting from the discussion section.

*The highlighting has been removed from the discussion section, however we strongly recommend that some part of the video include a brief montage of users manually segmenting, auto-segmenting in virtual reality, and applying stereology to the datasets as these aspects of data-analysis are not well represented in the literature. The purpose of the highlighted portions of the discussion were to provide examples of how the datasets produced using this protocol are effectively analyzed (Previously highlighted text: ...the image processing package Fiji for ImageJ... the software Reconstruct... The Amira Software... The software syGlass... Stereology generally consists of applying geometric grids to random, uniformly sampled images...).*

10. Please ensure that the references appear as the following: [Lastname, F.I., LastName, F.I., LastName, F.I. Article Title. Source. Volume (Issue), FirstPage–LastPage (YEAR).] For more than 6 authors, list only the first author then et al. Do not abbreviate journal names.

*The references have been proofread and fixed where necessary, the required JoVE reference style was used to format the manuscript references.*

---

### **Reviewers' comments:**

#### **Reviewer #1:**

Manuscript Summary:

This method article describes the most commonly used and well known protocol of Deerinck et al for SBF-SEM. This protocol is used in the majority of SBF-SEM articles and known by all the community. In a second part, this article presents unique imaging parameters as used in the Tescan SEM with a Gatan 3View. It describes how sample can be mounted and imaged. in a third part, authors are showing convincing examples nicely presented of scientific questions solved with their SBF-SEM.

Major Concerns:

-the structure of the article is not clear. A large part of the discussion describes the results of the protocol and should be in results. Many key findings are only presented in figure legends.

*We thank the reviewer for this comment, a large portion of the discussion has now been added to the results section making room for more in-depth discussion of reviewers' questions and comments in the discussion portion of the manuscript.*

-the references are insufficient and missing. A major revision of references should be done. Many discussions points are documented in literature and should be cited.

*We thank the reviewer for this comment, a major revision of the manuscript references has been completed.*

- For example, this protocol must be properly referenced at the beginning of the article and not in

discussion (reference 9) as Deerinck et al. (Enhancing Serial Block-Face Scanning Electron Microscopy to Enable High Resolution 3-D Nanohistology of Cells and Tissues July 2010 Microscopy and Microanalysis 16:1138-1139 DOI: 10.1017/S1431927610055170) with small modifications. As it is used in tens of publications, it should be mentioned with some key references. Particularly relevant for this article: He Q et al, Scientific reports, 2018.

*We thank the reviewer for this comment, the Deerinck paper is now explicitly mentioned and referenced in the introduction of the manuscript. The article by He Q et al. has been reviewed and integrated alongside additional key references throughout the manuscript.*

- Imaging parameters as used in this article are completely new to this field. It is really interesting and should be discussed more critically. There is no reported studies in the field where a dwell time as slow as 32 microsec/pixel was necessary to my knowledge. The most recent studies are between 1-5 microsecond/pixel. With all the other brands of microscope, SBF-SEM is done between 1 and 3 kV as higher beam accelerating voltage is damaging tissue and/or reduces resolution due to deep penetration depth of electrons. idem for z thickness.. Such imaging parameters are not transferable to any other SBF-SEM set-ups available on other brands of microscopes. A reference current measured with a Faraday cage should allow better comparisons between systems.

*We are glad to have piqued the interest of the reviewer with our imaging parameters, and thank the reviewer for this comment. The discussion has been expanded to comment on the parameters more critically. We would also like to thank the reviewer for calling attention to a mistake in the original manuscript which has now been corrected. During serial sectioning, a pixel dwell time of 12 microsec/pixel is used, serial imaging can then be paused at regions of interest to capture higher magnification/resolution images at a capture speed of 32 microsec/pixel. This is now discussed within the manuscript. We see no reason why the addition of carbon black, reduction of working distance, and application of silver paint and gold sputtering to the block would not result in these imaging settings being transferable to any other SBF-SEM set-up in order to capture high-quality images at 100-200 nm section thickness.*

Minor Concerns:

Figures 1-3 have the labels overlaid with the data

*We thank the reviewer for this comment, the error bars have been simplified across all figures in order to reduce overlays with the data.*

Fig 1 will gain in clarity and impact if the differences between the rows are visible on the figure itself

*We thank the reviewer for this comment, the figure has been modified to be more informative.*

Fig 2: real photos of the three steps will make it clearer

*We felt it would be more beneficial to show an ideal example of each step, best represented with an illustration, due to the video that JoVE will produce to accompany the protocol. We have highlighted the steps in question for inclusion in the video that will accompany the manuscript, so real examples of each step will be available to readers within the video along with close-ups of how each step is accomplished.*

Fig 9 rendering instead of rendition

*We thank the reviewer for this comment, the change has been made.*

Fig 9D rendering to be improved for clarity

*The legend discussing figure 9D has been expanded in order to provide further context and clarity for the*

*3D reconstruction rendered.*

**Reviewer #2:**

Manuscript Summary:

The manuscript 'Serial Block-Face Scanning Electron Microscopy (SBF-SEM): Preparing and Imaging Biological Tissue Samples' describes a general procedure for SBF-SEM sample preparation and imaging. A general sample preparation protocol and sample mounting is described in high detail and different imaging parameters that need to be fine-tuned for good quality images are also presented. Finally, the authors provide the documentation of their standard image reconstruction and segmentation workflow. The manuscript is very well-written and practical steps are explained in great detail. The authors put forward a workflow that is applicable to several tissue sample types.

Major Concerns:

- The described method is presented as a general workflow for biological tissue samples and the impression is given that any biological sample/question for SBF-SEM can make use of this exact protocol. While it is an excellent starting point, it is important to highlight that for each specific project it is worthwhile to optimize this further.

*Text has been added to the introduction to address this consideration.*

- Certain steps are device specific and presented here as settings that can be generally applied. Where appropriate, the text should be adjusted and it should be mentioned which steps or settings are general, which are specific for this device.

*Text has been added to inform the reader that imaging settings used were developed on our specific system.*

Minor Concerns:

- The authors bring up addition of heavy metals to the sample and silverpaint coating as steps to avoid electron charging artefacts. Since a few years, the use of an FCC (focal charge compensator) has been a solution to these charging artefacts. Although this may not be applicable to the device used here, the FCC should be mentioned in the discussion.

*The use of FCC devices has been included in the manuscript discussion.*

- The authors do not state whether their system is variable pressure (VP) or only operates under high vacuum.

*This information has been included in section three of the protocol.*

- Line 68 - 72: This phrase suggest that SBF-SEM will only work in a VP system. This should be adjusted, since there is mainly an increase in 3view intallations on high vacuum systems.

*We thank the reviewer for this comment, this section has been updated so that it does not suggest SBF-SEM only works on VP systems. The purpose of this section was to provide historical context for SBF-SEM and not to suggest a limitation. The text has been updated to include the use of high vacuum systems.*

- Step 1.8 line 146: Explain why this step is performed in the dark?

*We thank the reviewer for this comment, additional text stating that osmium tetroxide can be reduced by light has been added.*

- References to Figure 1: It is not clear from the text that the figure represents images after the step that was just described. Should be specified.

*We thank the reviewer for this comment, the figure legend has been updated to better describe which steps were included in each image and text has been added to the image for clarity.*

- Step 2.15, line 287-290: Please elaborate on the use of silverpaint around the sample and effect on damaging the diamond knife.

*The silver paint portion of the protocol has been expanded to elaborate on the application of silver paint to the sample, as well as touch on the concept of managing the longevity of the diamond knife. Step 2.13 has been updated to reflect this as well.*

- The HT settings of 7-12 kV are specific for the application on this device. Similar settings on another device (e.g. high vacuum Merlin) are not applicable. It should be highlighted in the text that this is a device specific recommendation.

*While the settings included in this manuscript are not widely used, there is no reason to believe that the kV settings used in this study would not work on another high vacuum device. The device used in this study was a Gatan 3View system installed in a Tescan microscope imaging under high vacuum. We have included text stating that the settings included were produced on our specific device, and the discussion has been expanded to touch on the novelty of our imaging settings.*

### **Reviewer #3:**

Manuscript Summary:

This protocol pertains to the preparation of biological samples (cornea and heart) for serial block-face imaging. The protocol covers all the steps to perform from the fixation to the imaging.

The article is very well written and the figures are well designed and informative.

Major Concerns:

Is the protocol applicable to the brain and other organs besides the cornea and heart? For the brain (for instance), it is best to perfuse the animals directly with the fixatives (as microglia are affected by drop-fixation).

*We thank the reviewer for this comment. We have applied this protocol to a number of tissues with a variety of fixation techniques and were too narrow in our scope when writing the original fixation step. It was our assumption that the individuals that would seek out this methods paper would be experienced EM users, most likely with experience in SEM or TEM work resulting in existing optimized fixation methods for their tissues of interest. It is always best to optimize fixation for the specific tissue and question being addressed, and as such we have rewritten the fixation step of this protocol to reflect this as well as to address the concept of fixation penetration.*

It would be best to mention cornea and heart in the article title, abstract and introduction to make sure the readers are aware that the protocol is applicable to the cornea and heart (in the different species examined).

*Text has been included to further expand the tissues and species to which this general method has been applied. Namely, this protocol has been applied to cornea and anterior segment structures, eyelid, lacrimal and herderian gland, retina and optic nerve, heart, lung and airway, kidney, liver, the cerebral cortex and medulla, and cremaster muscle, and in a variety of species including mouse, rat, rabbit, guinea pig, fish, monolayer and stratified cell cultures, pig, non-human primate, as well as human. It*

*would not be feasible to include figures from all tissue types and animal models we have applied this protocol to, however we have included what we believe are quality examples from a wide range of tissues and animals.*

In the different provided examples, what is the resolution (x-y-z)?

*We thank the reviewer for this question, the x-y-z resolution has been included in the figure legends of all reconstructions.*

Depending on resolution, different organelles and cell-cell interactions can be resolved.

The manuscript uses the term high-resolution. The exact range afforded with this technique should be mentioned.

*We thank the reviewer for this comment, protocol step 3.9 has been included in the manuscript to discuss resolution using this methodology.*

How is the 3D rendering performed?

*We thank the reviewer for this question and we agree that this would be useful information to include in the manuscript. A section has been included in the discussion of the paper discussing tips for the rendering of 3D reconstructions as well as introducing good-practices that aid in the reconstruction process.*

Minor Concerns:

1.1. How big should be the tissue samples at the beginning of the protocol? This information would be important considering that the penetration rate of fixatives is approximately 1mm per hour.

Can this protocol be applied to any type of biological tissue? What is the pH of the sodium cacodylate buffer? How is it prepared? The 'repeat tissue fixation' phrase is not clear (to me).

*We thank the reviewer for this comment, the fixation steps of the protocol have been rewritten to provide more detail and to better accommodate a variety of study designs. The size of tissue samples has been included, and the "repeat tissue fixation" phrase has been removed, as it is better covered in the extra provided details. The pH of the sodium cacodylate buffer and its method of preparation has been included.*

1.2. Are the washes at room temperature? How is the solution prepared and what is the pH?

*This information has been added to the manuscript.*

1.3. The same here, more information regarding how to prepare the solutions would be required.

*This information has been added to the manuscript.*

1.10. How is the uranyl acetate prepared?

*This information has been added to the manuscript.*

1.16 and 1.17. Are the incubations in resin performed at room temperature?

*The resin-embedding steps in 1.16 and 1.17 should occur at room temperature, this has been added to the manuscript text.*

2.15. What is the approximate ratio of acetone to silver?

*As acetone evaporates rapidly, the approximate ratio is difficult to state accurately. It is more appropriate to state a desired consistency. However, to provide further direction when applying acetone the text has been updated to reflect this.*